

## Article

# Analysis of the Influence of Silty Sands Moisture Content and Impact Velocity in SHPB Testing on Their Compactability and Change in Granulometric Composition

Kamil Sobczyk , Ryszard Chmielewski , Leopold Kruszka  and Ryszard Rekucki

Department of Military Engineering and Military Infrastructure, Faculty of Civil Engineering and Geodesy, Military University of Technology, 2 Gen. Sylwester Kaliski Str., 00-908 Warsaw, Poland; ryszard.chmielewski@wat.edu.pl (R.C.); leopold.kruszka@wat.edu.pl (L.K.); ryszard.rekucki@wat.edu.pl (R.R.)  
\* Correspondence: kamil.sobczyk@wat.edu.pl

**Abstract:** This paper presents the results of a test cycle of two types of silty sand (*siSa*) with different contents of fine fractions. Fine fractions are understood as soil grains with a grain diameter of less than 63  $\mu\text{m}$  (as the sum of silt and clay fractions). The soils tested had a content of fine fractions of  $f_{Si+Cl,1} = 15.14\%$  and  $f_{Si+Cl,2} = 20.48\%$ , respectively, before the study. Changes in the content of these fractions after the experiments were analyzed. These experiments consisted of dynamic bar projectile impact loading, and a split Hopkinson pressure bar (SHPB) test stand was used in the study. Changes in the granulometric composition of the silty sands studied were carried out in a laser particle size analyzer, allowing measurement of fractional content in the grain size range from 0.01  $\mu\text{m}$  to 3500  $\mu\text{m}$ . As a result, a summary of changes in soil grain size curves in the range of fine fractions was compiled. Repeated trends were observed in the changes in the granulometric composition of the soil samples as a function of the moisture content of the soil sample ( $w_1 = 0\%$ ,  $w_2 = 5\%$ ,  $w_3 = 10\%$ , and  $w_4 = 15\%$ ) and the impact velocity of the loading bar projectile for SHPB pneumatic launcher pressures ( $p_1 = 1.2 \text{ bar} \rightarrow v_1 = 12.76 \text{ m/s}$ ,  $p_2 = 1.8 \text{ bar} \rightarrow v_2 = 17.69 \text{ m/s}$  and  $p_3 = 2.4 \text{ bar} \rightarrow v_3 = 21.32 \text{ m/s}$ ). The influence of the initial moisture content of the investigated soil on the value of the optimum moisture content obtained during its dynamic compaction was discussed. The trend in the behavior of the change in the granulometric composition of the tested samples was determined, taking the value of the initial moisture content of the soil in relation to the optimum moisture content of the reference sample as a reference. The largest percentage change in granulometric composition through an increase in the value of the silt and clay fraction relative to the reference sample  $f_{Si+Cl}$  for both types of silty sand tested occurs for the same moisture content variant  $w_2 = 5\%$ —for soil  $f_{Si+Cl,1} = 15.14\%$  there is an increase in the fine fraction of 11.08% and for soil  $f_{Si+Cl,2} = 20.48\%$  there is an increase in the fine fraction of 15.17%. In general, it can be seen that more silty soil is more strongly susceptible to the phenomenon of grain crushing for moisture content  $w_1 = 0\%$  and  $w_2 = 5\%$  less than its optimum moisture content  $w_{opt,1} = 8.70\%$ . In contrast, less silty soil is more susceptible to the phenomenon of grain crushing for moisture contents  $w_3 = 10\%$  and  $w_4 = 15\%$  greater than its optimum moisture content  $w_{opt,2} = 9.20\%$ . The presented dynamic physical phenomenon of soil behavior is crucial during explosive and impact impacts on structures made of soil, e.g., as ground protection layers.



**Citation:** Sobczyk, K.; Chmielewski, R.; Kruszka, L.; Rekucki, R. Analysis of the Influence of Silty Sands Moisture Content and Impact Velocity in SHPB Testing on Their Compactability and Change in Granulometric Composition. *Appl. Sci.* **2023**, *13*, 4707. <https://doi.org/10.3390/app13084707>

Academic Editor: Jong Wan Hu

Received: 14 March 2023

Revised: 1 April 2023

Accepted: 6 April 2023

Published: 8 April 2023



**Copyright:** © 2023 by the authors. Licensee MDPI, Basel, Switzerland. This article is an open access article distributed under the terms and conditions of the Creative Commons Attribution (CC BY) license (<https://creativecommons.org/licenses/by/4.0/>).

**Keywords:** granulometric composition; grain crushing; laser particle size analyzer; silty sand; soil; high strain rate; split Hopkinson pressure bar

## 1. Introduction

Issues related to the behavior of different materials subjected to dynamic impact using a split Hopkinson pressure bar test stand are an important part of impact engineering. For many years, there has been an unflagging interest and continuous development

in the area of experiments on the dynamic mechanical properties of various structural materials, including building materials—the materials studied include metals [1–3], polymers [4–6], concrete [7–9], reinforced composites [10–12], wood [13–15], rocks [16–18] and, more recently, soils [19–22]. Soils are used as an energy-absorbing material during explosive and impact impacts on structures as ground protective layers for these structures. The intensification of research has also been accompanied by an increase in publications on the subject of modifying the specimen variants used and the experimental conditions associated with the Hopkinson bar technique. A summary of the conducted dynamic research, together with the construction and description of the SHPB test stand, has been collected in several review articles [23–25]. Table 1 shows a comparison of the total number of scientific papers (research and review article, book chapter, conference paper) using “Hopkinson bar” as a keyword between 2018 and 2022 according to the resources of the scientific databases Web of Science and Springer Link.

**Table 1.** Summary of the total number of scientific papers (research and review article, book chapter, conference paper) using “Hopkinson bar” as a keyword concerning dynamic experiments with samples of different materials from 2018 to 2022 according to the resources of the scientific databases Web of Science and Springer Link [26,27].

Year	Web of Science	Springer Link
2022	592	587
2021	538	456
2020	510	351
2019	486	359
2018	447	321

Directly related to the conduct of dynamic experiments based on the SHPB test stand is the issue of the effect of loading rate on changes in the microstructure of the tested sample—the group of structurally sensitive materials to dynamic effects includes brittle materials: rocks [28–30], coal [31,32], and loose material, e.g., non-cohesive soils [33–36]. Particularly valuable are the analyses and conclusions of published dynamic SHPB studies conducted for concrete samples [37] and different types of sand—coral sand [38] and calcareous sand [39]. Issues related to these analyses of the grain size change as the effect of particle size distribution on dynamic properties of different types of sand, e.g., calcareous sand and coral sand [40–42]. The mechanical behavior of different types of sand is strongly related to the particle size of the grains in its soil skeleton. In the reviewed papers, studies were conducted to investigate the effect of particle size distribution on the impact resistance of samples of different sand types based on SHPB dynamic tests. The results of the study were interpreted that sands (e.g., coral sand) experienced a very strong and sudden increase followed by a slow, gradual decrease in impact resistance with increasing average particle size  $d_{50}$  and cohesion  $c$ . Sands of different grain sizes had concretely apparent different force transmission mechanisms and failure patterns. When the particles were uniformly distributed, strength was provided by an arrangement of particles with the correct diameter and with cohesion  $c$  resulting from the fine fraction. Strength decreased when particle breakage occurred, and the force transmission mechanism changed, which also led to an uneven particle size distribution process.

The subject of this article is a non-cohesive soil–silty sand. It is often used as a backfill soil, i.e., an explosion-absorbing material in protective construction. The effect of dynamic action on loose soil–silty sand can be characterized by comparative analysis of the individual fractions in the soil structure (in particular, consider sandy fractions  $f_{Sar}$ , silty fractions  $f_{Si}$ , and clay fractions  $f_{Cl}$ ). A schematic division of the soil fractions according to [43] is shown in Figure 1.

Cl	Si			Sa			Gr			Co
	FSi	MSi	CSi	FSa	MSa	CSa	FGr	MGr	CGr	
	0,002	0,0063	0,02	0,063	0,2	0,63	2	6,3	20	63
	[mm]									

**Figure 1.** Schematic division of soil fractions (adapted from Ref. [43]). Orange and green colors indicate the key range of silt fraction  $f_{Si}$  and clay fraction  $f_{Cl}$  in this article together with the limiting grain size diameters.

Testing the grain size distribution of non-cohesive soils is carried out by determining the granulometric composition using the laboratory sieve method according to [44]. The smallest mesh diameter of the sieve is 0.063 mm (63  $\mu\text{m}$ )—in order to gain a more accurate understanding of the further course of the grain size curve in the range below 63  $\mu\text{m}$ , it is necessary to use precision laboratory equipment, as aerometric analysis for small soil samples is not feasible. In this study, a laser particle size analyzer was used to produce a more detailed grain size curve from a grain size of 0.01  $\mu\text{m}$  to 3500  $\mu\text{m}$ —additional grain size curve data in the range of 0.01–63  $\mu\text{m}$  can be obtained in comparison with classic sieve analysis (gradation test).

Sand, as a natural granular material, is a complex non-equilibrium energy dissipating system requiring detailed analyses. This is the motivation of the authors of the manuscript to add to the wide area of already existing publications on different sands the results of dynamic studies for one type of sand—silty sand (there is still a space of insufficiently studied examples of these soils). The aim of this study was to investigate the change in the granulometric composition of silty sand (two soil types— $f_{Si+Cl,1} = 15.14\%$  and  $f_{Si+Cl,2} = 20.48\%$ ) in dynamic SHPB experiments with varying moisture content— $w_1 = 0\%$ ,  $w_2 = 5\%$ ,  $w_3 = 10\%$  and  $w_4 = 15\%$ —and the impact velocity of the loading bar projectile for SHPB pneumatic launcher pressures— $p_1 = 1.2$  bar ( $v_1 = 12.76$  m/s),  $p_2 = 1.8$  bar ( $v_2 = 17.69$  m/s), and  $p_3 = 2.4$  bar ( $v_3 = 21.32$  m/s).

Major points of highlights and innovations of study in this paper:

- Use of laser particle size analyzer to determine the grain size composition of the soil sample (grain size curve)—a more accurate method due to the wide range of possibilities for 0.01  $\mu\text{m}$  to 3500  $\mu\text{m}$  grain diameters testing compared to classic sieve analysis (gradation test) and aerometric analysis methods.
- Two types of silty sand with different contents of fine fractions were used for the study— $f_{Si+Cl,1} = 15.14\%$  and  $f_{Si+Cl,2} = 20.48\%$ . The manuscript also has a practical (not only academic) aspect because the two types of silty sand studied were from the construction site of two different construction critical infrastructure facilities in Poland—the soil samples taken were really existing in the subsoil.
- The study was conducted for a number of variants of soil samples depending on the variables, the impact velocity of the loading bar projectile for SHPB pneumatic launcher pressures, and moisture content of the sample (below and above the optimum moisture content) in order to create several potential sets of conditions for the use of this soil as, for example, ground protection layers loaded by dynamic action.
- Repeatable trends in changes in the granulometric composition of soil samples were observed and shown graphically on grain size curves. The largest percentage change in granulometric composition through an increase in the value of the silt and clay fraction relative to the reference sample  $f_{Si+Cl}$  for both types of silty sand tested occurs for the same moisture content variant  $w_2 = 5\%$ —for soil  $f_{Si+Cl,1} = 15.14\%$ , there is an increase in the fine fraction of 11.08%, and for soil  $f_{Si+Cl,2} = 20.48\%$ , there is an increase in the fine fraction of 15.17%.

## 2. Characteristics of Soil Samples

In this study, two different types of non-cohesive soil samples were analyzed—two samples of silty sand with different percentages of fine fractions (silt and clay) in the soil skeleton. The silty sand is an example of a poorly expansive soil (doubtful soil—ambiguous

expansivity) and belongs to the group of soils between expansive and non-expansive soils (using the expansivity criterion according to Wilun). The criteria for soil freeze–thaw effects depend on the physical properties of the soil. Non-cohesive soils with a low silt and clay fraction do not form freeze–thaw effects even when saturated with water. The ice that forms in them presses excess water downwards so that these soils contain less water in the pores after freezing than before. Cohesive soils, on the other hand, which contain more silty particles, are more expansive; the finer the grain size, the higher the moisture content. The finer the grain size of the soil, the greater its moisture content. The finer the grain size of the soil, the smaller the pore size, and the more pores are almost completely filled with adsorbed water, the better the conditions for the formation of separated ice lenses and the formation of freeze–thaw effects. Poorly expansive soils (also referred to as doubtful soils) contain about 20–30% of particles smaller than 0.05 mm and about 3–10% of particles smaller than 0.002 mm [45–47]. Table 2 shows the accepted general division of soils into four groups in terms of their susceptibility to the phenomenon of freeze–thaw effects [48].

**Table 2.** General classification of soil types with regard to the phenomenon of freeze–thaw effects (symbols of soil names according to [43]).

Group I Non-Expansive Soils	Group II Poorly Expansive Soils (Doubtful Soils)	Group III Expansive Soils	Group IV Very Expansive Soils
Gravel (Gr)	silty sand (siSa)	sandy-silty clay (sasiCl)	clayey sand (clSa)
sand-gravel mix (grSa)	clayey gravel (clGr)	clay (Cl)	sandy silt (saSi)
coarse sand (CSa)	clayey sand-gravel mix (grclSa)	sandy clay (saCl)	silt (Si)
medium sand (MSa)		silty clay (siCl)	clayey silt (clSi)
fine sand (FSa)			

Samples of silty sand with different silt and clay fraction contents were used in the research within the scope of this article. In order to correctly analyze the change in the granulometric composition of the silty sand, a key step is to determine the initial grain size structure for the reference samples. A state-of-the-art laser particle size analyzer Bettersizer S3 Plus was used in the study in the wet soil sample variant—a detailed description of the test methodology is presented in Section 3. As a result of the analysis, graphs of grain size curves were determined, and the content of the silt and clay fraction (understood as the percentage of grains with a diameter of less than 63  $\mu\text{m}$ ) was found to be equal for the:

- first type of soil sample— $f_{Si+Cl,1} = 15.14\%$  (the grain size curve in Figure 2a);
- second type of soil sample— $f_{Si+Cl,2} = 20.48\%$  (the grain size curve in Figure 2b).

Figure 3 shows the macroscopic appearance of the two reference samples of silty sand. Visually comparing them to each other, it is not possible to visually identify them due to the small grain diameter size in the silt and clay fractions—macroscopically, the samples appear similar.

Both types of samples were analyzed in the optimum moisture content test (Proctor apparatus) according to [49]. The value of the optimum moisture content  $w_{opt}$  was determined for the obtained maximum volumetric density of the soil skeleton  $\rho_{d,max}$ , at constant compaction energy and for different moisture contents:

- for  $f_{Si+Cl,1} = 15.14\%$ — $\rho_{d,max,1} = 1.89 \text{ g/cm}^3 \rightarrow w_{opt,1} = 8.70\%$  (Figure 4a);
- for  $f_{Si+Cl,2} = 20.48\%$ — $\rho_{d,max,1} = 1.95 \text{ g/cm}^3 \rightarrow w_{opt,2} = 9.20\%$  (Figure 4b).

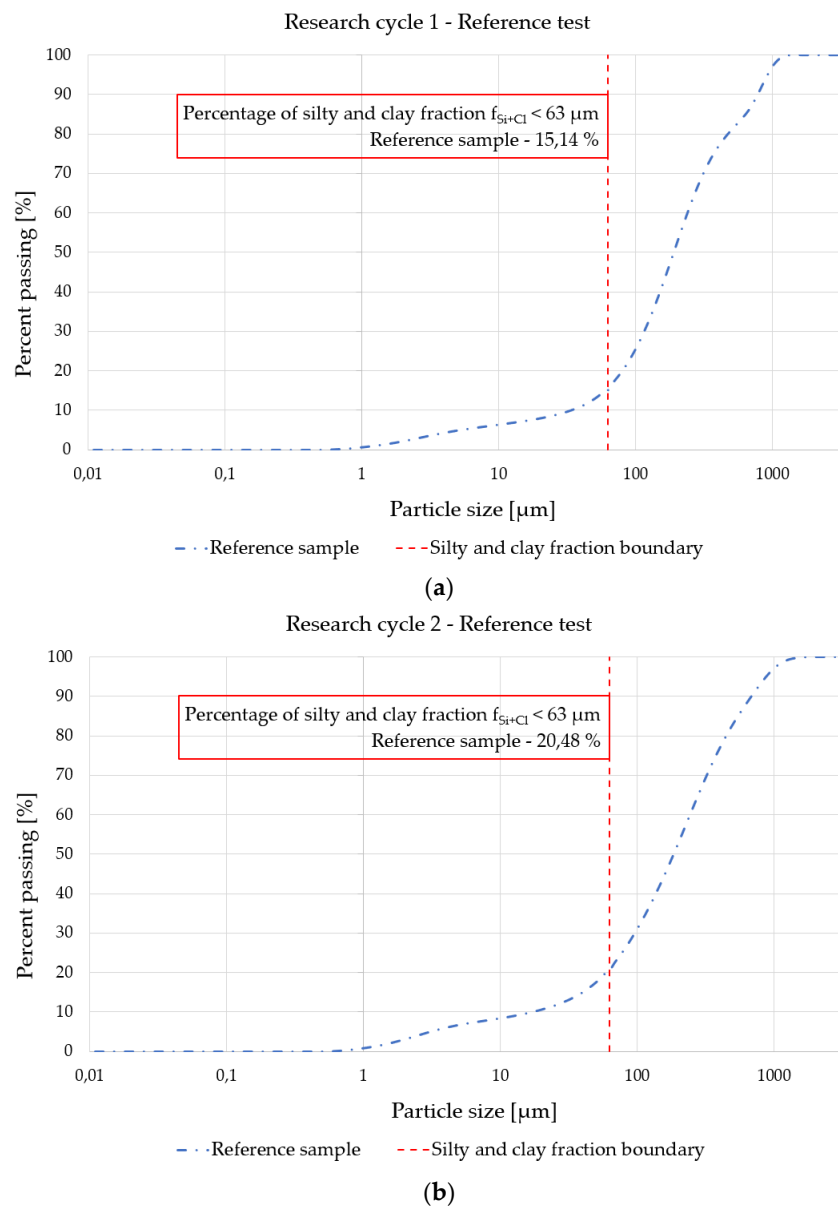


**Figure 2.** Comparison of graphs of grain size curves for silty sand with silt and clay fractions: (a)  $f_{Si+Cl,1} = 15.14\%$  and (b)  $f_{Si+Cl,2} = 20.48\%$ .

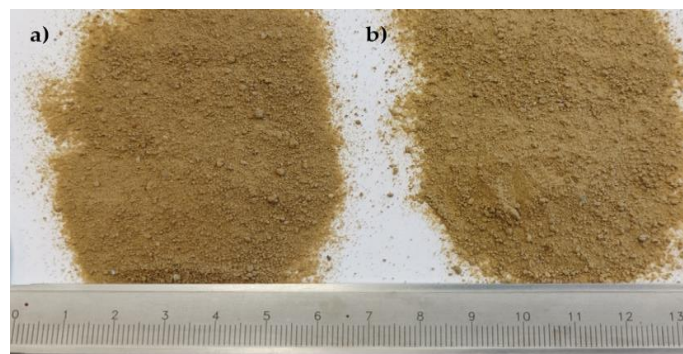


**Figure 3.** Macroscopic view comparison of reference silty sand samples: (a)  $f_{Si+Cl,1} = 15.14\%$  and (b)  $f_{Si+Cl,2} = 20.48\%$ .

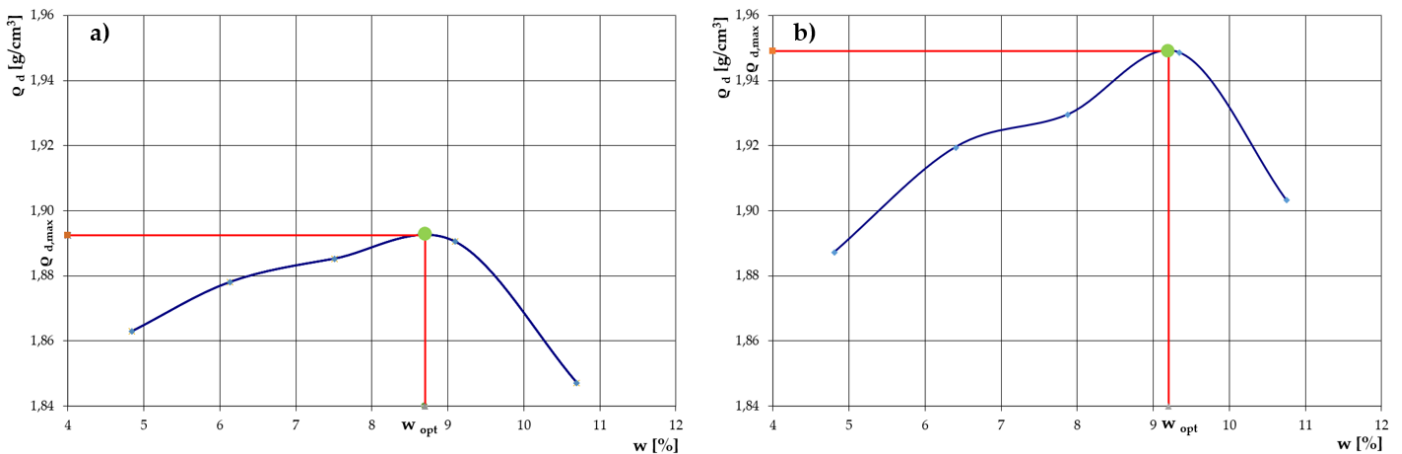


**Figure 4.** Comparison of optimum moisture content  $w_{opt}$  for samples: (a)  $f_{Si+Cl,1} = 15.14\%$  and (b)  $f_{Si+Cl,2} = 20.48\%$  (the blue line is the volumetric density curve of the soil in relation to its moisture content, the red line is the horizontal drop from the Y axis of the maximum volumetric density value of the soil and the vertical drop to the X axis (moisture content) to determine the optimum moisture content, the green color indicates the point of inflection of the curve of the graph).

### 3. Test Stand and General Experimental Methodology

#### 3.1. Description and Components of the Test Stand

Once the soil sample has reached the laboratory, the testing analysis process is carried out on various test stands, including macroscopic evaluation of the physical properties of the soil or determination of the optimum moisture content (Proctor apparatus). In accordance with the subject of this article, the main test stands used in the experiment include a split Hopkinson pressure bar (SHPB) and a laser particle size analyzer.

The SHPB test stand takes into account the known density, moisture content, and strain rate of the granular structure of the soil sample in order to determine the dynamic properties of the soil being analyzed and to understand the stress–strain relationship. The main essence of the Hopkinson technique is that it is possible to analyze the response of different materials (including soil samples) subjected to dynamic action. The dynamic tests, the effect of which is the main focus of this work, were carried out based on the SHPB test stand located in the Department of Military Engineering and Infrastructure in the Faculty of Civil Engineering and Geodesy, MUT. A schematic diagram of the SHPB is shown in Figure 5, and an actual view of the test stand is in Figure 6.

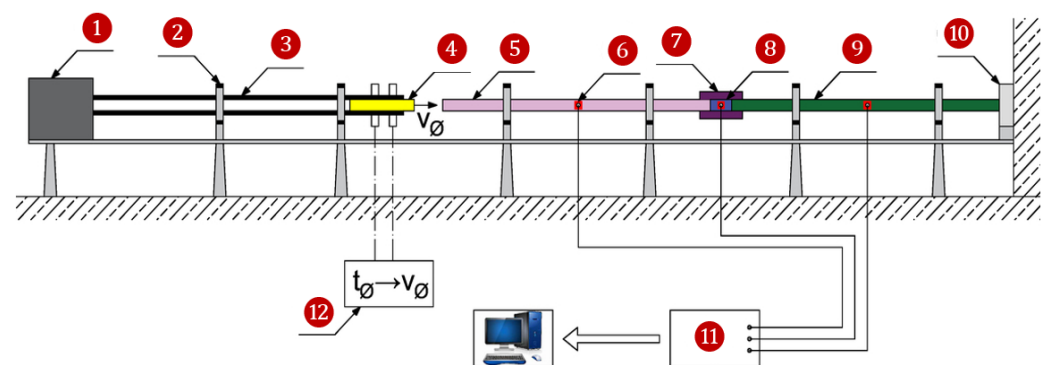


**Figure 5.** SHPB test stand diagram with designations of important components 1–12 (reprinted from Ref. [50]).

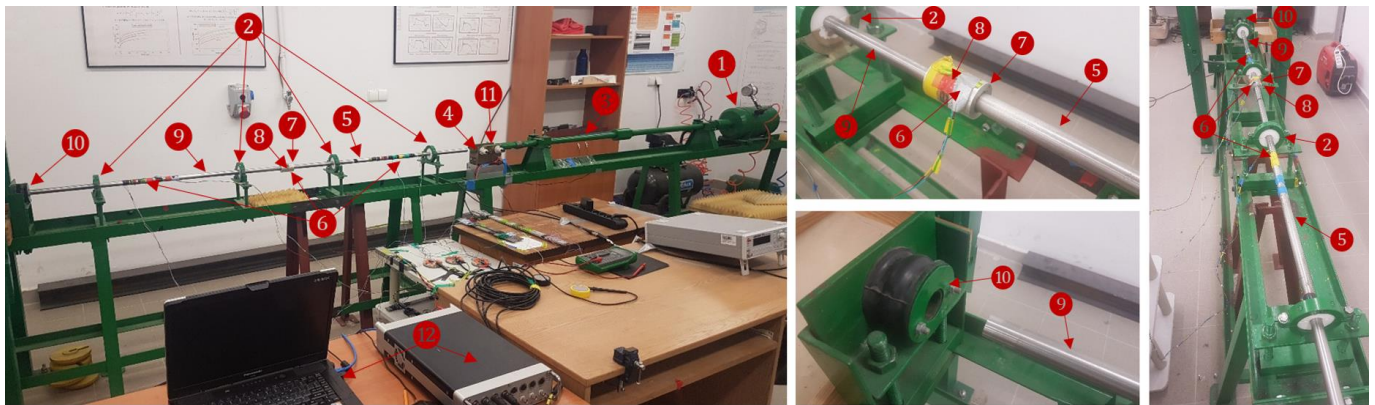


**Figure 6.** View of the SHPB test stand located in the Department of Military Engineering and Infrastructure of the MUT, with markings of crucial components ①–⑫.

The following components of the SHPB test stand can be distinguished as important due to the specifics of the dynamic experiment methodology:

- ①—pneumatic bar projectile launcher [51];
- ②—design to ensure that the bars are axially aligned with each other;
- ③—bar projectile guide (launcher barrel);
- ④—bar projectile;
- ⑤—initiating bar;
- ⑥—set of measuring strain gauges;
- ⑦—soil sample casing (rigid ring);
- ⑧—soil sample under test;
- ⑨—transmitting bar;
- ⑩—damper (impact-absorbing element);
- ⑪—bar projectile speed measurement kit  $v_0$ ;
- ⑫—digital recorder with computer.

The Bettersizer S3 Plus laser particle size analyzer was used to investigate the granulometric composition for each soil sample variant. The instrument combines the measurement methods of static light scattering and dynamic image analysis, thus offering the versatile ability to characterize particle size and shape in the range from 0.01  $\mu\text{m}$  to 3500  $\mu\text{m}$ . Analyses of changes in the granulometric composition of silty sand samples (as a result of dynamic bar projectile interaction within the SHPB stand experiments) were carried out based on the wet version of the grain size curve study in the Bettersizer S3 Plus laser particle size analyzer—the device is shown in Figure 7. It is located in the Department of Engineering and Military Infrastructure in the Faculty of Civil Engineering and Geodesy, MUT.

Important components of the laser particle size analyzer include:

- ①—main analyzer core;
- ②—measuring chamber system (water–soil mixture input–output);
- ③—circulation tank;
- ④—circulation and dispersion system of the water–soil mixture;
- ⑤—distilled water tank;
- ⑥—computer with dedicated software.



**Figure 7.** View of the Bettersizer S3 Plus laser particle size analyzer test stand located in the Department of Military Engineering and Infrastructure of the MUT, with markings of crucial components ①–⑥.

### 3.2. General Methodology for Conducting the Experiment

The soil sample ⑧ of the SHPB test is cylindrical in shape and is placed in a rigid casing ⑦ made of different materials depending on the experimental setup, e.g., Plexiglas, duralumin, or steel. The dimensions and material characteristics of the casing ensure that the uniaxial deformation state of the tested soil occurs when the specimen is pressed from both sides by the initiating ⑤ and transmitting ⑨ bars. According to the markings in Figure 6 and the methodology for conducting the SHPB experiment, the bar projectile load ④ is propelled inside the bar projectile guide ⑥ by rapidly released air pressure from a pneumatic launcher ①. The laser timing system ⑩ takes a reading of the time it takes for the bar projectile to move a known distance. Knowing this time allows the impact velocity to be determined. When the bar projectile strikes the initiating bar ⑤, a compressive elastic wave is generated in the bar (the incident wave generates deformations in the initiating bar  $\epsilon^I$ ), propagating along the bar toward the soil sample ⑧ surrounded by the casing element (rigid ring) ⑦. On reaching the end of the initiating bar, the wave partly continues to propagate (the transmitted wave generates deformations in the transmitting bar  $\epsilon^T$ ) through the sample towards the transmitting bar and partly is reflected and starts to return to the beginning of the initiating bar (the reflected wave generates deformations in the initiating bar  $\epsilon^R$ ). The wave that has passed through the sample and reached the transmitting bar at its end is finally attenuated in the damping element ⑩. The signals from the set of measuring strain gauges are recorded by a digital recorder and transmitted to a computer ⑫.

The investigation in the laser particle size analyzer (Figure 7) begins by flushing the unit system and pumping a new portion of the liquid from the distilled water tank ⑤ into the circulation tank ③. Once the soil sample has been transferred to the circulation tank ③, the water–soil mixture flows through the circulation and dispersion system ④. During the measurement, the particles dispersed in the selected medium are pumped through a set of two measuring chambers ② within the main core of the analyzer ①. In the first measuring chamber, short-wave laser light (532 nm) passes through the sample and is scattered according to the particle size. The 96 detectors detect optical signals over an angle range of 0.02–165°. Meanwhile, in the second measurement cell, CCD cameras (with 0.5× and 10× magnification) continuously take images to provide particle image analysis in the range of 2 μm to 3500 μm. An additional lens between the laser and the sample cell (lens 2) converts the diverging laser beam into a parallel beam and enables the detection of back-scattered light. The evaluation of the fine particle size distribution is based on the Fraunhofer or Mie scattering theory, which depends on the particle size and optical properties. Mie scattering theory enables an accurate

description of the laser scattering law of particles—it is a widely accepted theory in modern laser particle size analysis. Fraunhofer diffraction theory is a simplified version of Mie theory—relatively rarely used, mainly applied to describe the laser scattering law of relatively coarse particles. Mie theory is adopted for all bulk materials over a wide range of grain diameters. The Fraunhofer method is more dedicated to the analysis of coarse-grained powders. In the present work, Mie theory is adopted for further analysis. The methodology described is in accordance with the ISO standards on the subject [52–54]. Figure 8 shows a detailed scheme of particle size testing by laser diffraction from the stage of introduction of a soil sample into the system to the stage of analysis of the obtained results in dedicated computer software.

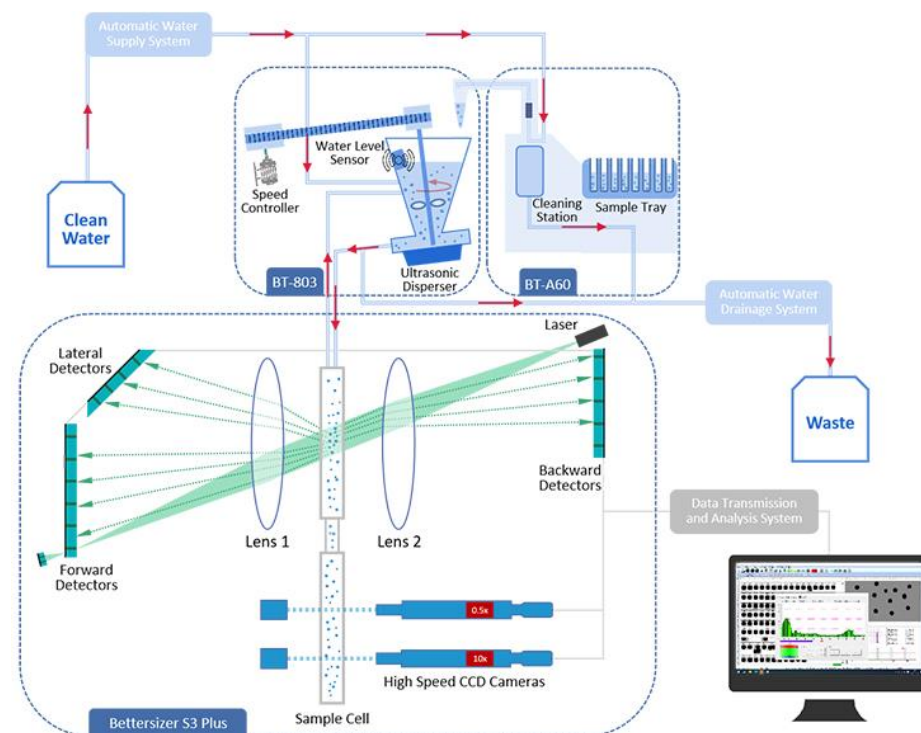


**Figure 8.** Detailed diagram of a soil sample test procedure on the Bettersizer S3 Plus laser particle size analyzer located in the Department of Military Engineering and Infrastructure of the MUT (reprinted from Ref. [55]).

### 3.3. Process of Preparing a Soil Sample for Testing

In the process of preparing a non-cohesive soil sample for dynamic testing using the SHPB test stand, an important step is to ensure the initial compaction state of the soil. In particular, this is an important step of the preparation process for dry and low moisture content samples. Such a sample is in a two-phase or three-phase state—it has a gas phase (usually in the form of air). Failure to carry out the compaction process will result in incorrect experimental results—some of the impact energy of the bar projectile will be used to compact the air voids.

The soil sample is cylindrical in shape, and its dimensions must comply with the condition [56] in Equation (1):

$$L = d \cdot \sqrt{\frac{3 \cdot \nu}{4}}; \quad (1)$$

where  $L$ —length of soil sample tested;

$d$ —diameter of soil sample tested;

$\nu$ —Poisson's ratio of soil sample tested.

Using approximations of the calculated values, it is possible to determine the general approximation condition [57] in Equation (2):

$$L \approx 0.5 \cdot d. \quad (2)$$

The diameter of the soil sample corresponds to the diameter of the bar projectile and the measuring bars (initiating and transmitting). The indicated elements of the SHPB test stand in the Department of Military Engineering and Infrastructure of the MUT have a diameter of 20 mm—based on Equation (2), the length of the soil sample is approximately 10 mm.

In the experimental methodology of SHPB testing, an important step is the selection of a suitable impulse shaper to ensure dynamic stress equilibrium. The introduction of an additional impulse shaper into the SHPB test stand system between the bar projectile and the initiating bar allows for a longer time of rising impulse, which enables the effect of better impedance matching and homogeneous deformation of the test material. The pulse shaper is usually a small and thin disc made of soft material—it can be made of aluminum, brass, rubber, nylon, copper, or stainless steel, about 0.1–2 mm thick [58]. During testing, the bar projectile strikes the impulse shaper in front of the initiating bar, thus generating a non-dissipative impulse propagating through the initiating bar. This pulse, with its slowly rising front, facilitates dynamic balancing of forces on the sample—a slowly rising pulse is the preferred loading pulse to minimize the effects of dissipation and inertia, thereby facilitating dynamic stress balance in the sample. The task of the pulse shaper is to ensure a constant strain rate during loading and to maintain force balance throughout the specimen. By changing the geometry of the pulse shaper, a variety of different pulses incident on the specimen can be produced. Depending on the materials being tested, different loading pulses are needed, which can be achieved by designing the shaper accordingly. The dynamic stress equilibrium condition is shown in Equation (3):

$$\varepsilon^I(t) + \varepsilon^R(t) \cong \varepsilon^T(t); \quad (3)$$

where  $\varepsilon^I$ —initiated wave (incident impulse);

$\varepsilon^T$ —transmitted wave (transmitted impulse);

$\varepsilon^R$ —reflected wave (reflected impulse).

Taking into account the addition and negative signs of the  $\varepsilon^I$ ,  $\varepsilon^T$ , and  $\varepsilon^R$  graphs, it is possible to check the fulfillment of the dynamic stress equilibrium condition according to Equation (3) by comparing the changes in the course of the graphs. An example of such a graph is shown in Figure 9—it is possible to compare the correspondence of the course of the blue graph  $\varepsilon^I$  and the black graph with the dashed line  $\varepsilon^T - (-\varepsilon^R)$ , where final form is  $\varepsilon^T + \varepsilon^R$ .

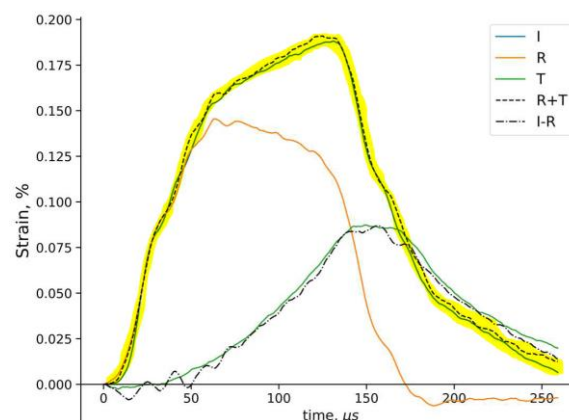


**Figure 9.** Example of graphical representation of the fulfillment of dynamic stress equilibrium condition (reprinted from Ref. [59]).

In accordance with the conclusions of the publication [60], the compaction process of the sample was carried out on a vibrating shaker. The soil was compacted by vibrating the shaker for 60 s. The tests carried out in [60] proved that a time of 60 s was sufficient—the vibration process for longer periods of 120 s and 180 s did not result in a significant increase in soil compaction values. A sinker weight of approximately 1000 g was applied to the sample to improve the effectiveness of the shaking compaction. During the shaker operation, the air voids were filled by the moving soil grains—the compaction process took place. Figure 10 shows the soil sample casing (rigid ring) and the auxiliary components necessary for the compaction process of a soil sample, with their markings:

- ❶—base cork;
- ❷—soil sample casing (rigid ring);
- ❸—sily sand sample;
- ❹—fixing screws;
- ❺—pressure plate;
- ❻—sinker 1000 g.

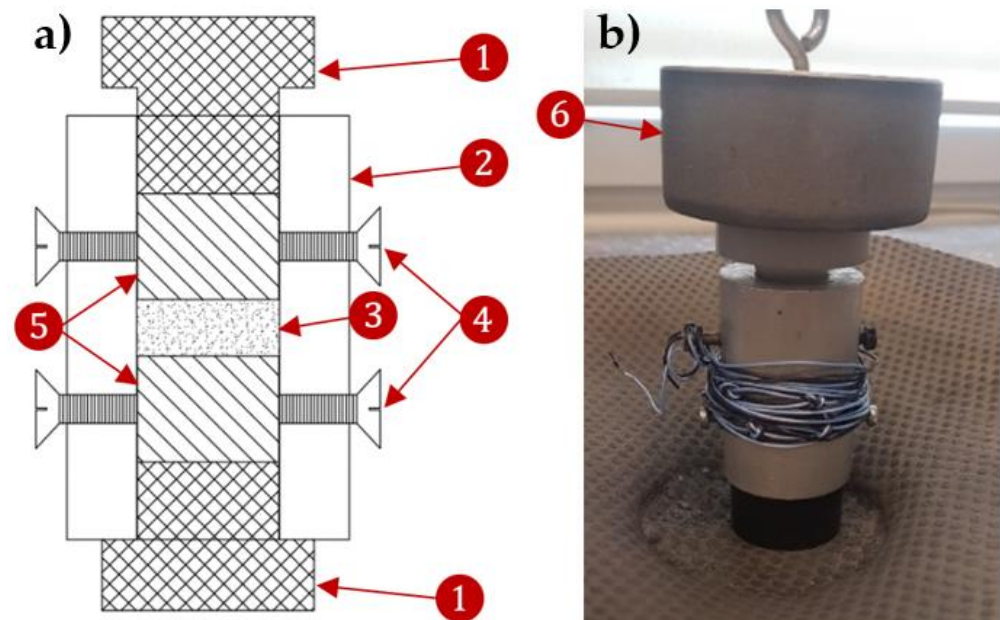


**Figure 10.** Installation for compaction of a sample of non-cohesive soil as part of the SHPB test with markings of the crucial components: (a) schematic diagram and (b) actual view ❶–❻ (reprinted from Ref. [60]).

The variant soil sample prepared in this way was subjected to a dynamic experiment on the SHPB test stand according to the methodology discussed in Section 3.2. The variants of the test sample distinguished in terms of the initial launcher pressure acting on the bar projectile  $p_i$  (i.e., determining the average impact velocity of the bar projectile  $v_i$ ) and the moisture content of the soil sample  $w_i$  (percentage of water in the sample) are summarized in Table 3. A total of 12 variants of the silty sand sample were distinguished. Each variant of the sample was dynamically tested 4 times to obtain a meaningful statistical sample for both variants of silty sand with a silt and clay fraction  $f_{Si+Cl,1} = 15.14\%$  and  $f_{Si+Cl,2} = 20.48\%$ —a final of 96 experiments were performed on the SHPB test stand.

The soil samples after the completed dynamic experiments were combined according to the distribution shown in Table 3, and a reference sample (a silty sand sample not subjected to dynamic impact in the SHPB test) was added to the compilation—a summary of the silty sand sample variants used in the laser particle size analyzer is shown in Table 4.

**Table 3.** Summary of silty sand sample variants used in experiments conducted on the SHPB test stand.

I	II	III	IV	V	VI	VII	VIII	IX	X	XI	XII
$w_1 = 0\%$			$w_2 = 5\%$			$w_3 = 10\%$			$w_4 = 15\%$		
$p_1 = 1.2$ bar $v_1 = 12.76$ m/s	$p_2 = 1.8$ bar $v_2 = 17.69$ m/s	$p_3 = 2.4$ bar $v_3 = 21.32$ m/s	$p_1 = 1.2$ bar $v_1 = 12.76$ m/s	$p_2 = 1.8$ bar $v_2 = 17.69$ m/s	$p_3 = 2.4$ bar $v_3 = 21.32$ m/s	$p_1 = 1.2$ bar $v_1 = 12.76$ m/s	$p_2 = 1.8$ bar $v_2 = 17.69$ m/s	$p_3 = 2.4$ bar $v_3 = 21.32$ m/s	$p_1 = 1.2$ bar $v_1 = 12.76$ m/s	$p_2 = 1.8$ bar $v_2 = 17.69$ m/s	$p_3 = 2.4$ bar $v_3 = 21.32$ m/s

Total sample variants: 12.

**Table 4.** Summary of silty sand sample variants used in particle size change analyses.

I	II	III	IV	V	VI	VII	VIII	IX	X	XI	XII	XIII
$w_1 = 0\%$			$w_2 = 5\%$			$w_3 = 10\%$			$w_4 = 15\%$			
$p_1 = 1.2$ bar $v_1 = 12.76$ m/s	$p_2 = 1.8$ bar $v_2 = 17.69$ m/s	$p_3 = 2.4$ bar $v_3 = 21.32$ m/s	$p_1 = 1.2$ bar $v_1 = 12.76$ m/s	$p_2 = 1.8$ bar $v_2 = 17.69$ m/s	$p_3 = 2.4$ bar $v_3 = 21.32$ m/s	$p_1 = 1.2$ bar $v_1 = 12.76$ m/s	$p_2 = 1.8$ bar $v_2 = 17.69$ m/s	$p_3 = 2.4$ bar $v_3 = 21.32$ m/s	$p_1 = 1.2$ bar $v_1 = 12.76$ m/s	$p_2 = 1.8$ bar $v_2 = 17.69$ m/s	$p_3 = 2.4$ bar $v_3 = 21.32$ m/s	Reference sample

Total sample variants: 13.

For each soil sample variant, 5 mini-samples of 0.2 g were extracted. This mass value is due to the specifics of the test in this model of the Bettersizer S3 Plus laser particle size analyzer—feeding a larger mass of soil sample causes a process of flushing the excess sample out of the circulation tank until the desired mass effect of approximately 0.2 g is achieved. Distilled water was added to each of the 5 vessels containing an equal variant of the sample. Over a period of 24 h, the sample underwent a process of disentangling and loosening the clumps of the silt and clay fraction. The combined silt and clay particles (soil aggregate) were separated in the water into individual soil particles. After waiting for 24 h and the particle separation process, the soil sample was transferred to the circulation tank together with the water in the vessel. The remaining sediment in the vessel was also washed into this circulation tank—this ensures that no soil grains remain on the vessel walls. The laser particle size analysis was then commenced according to the methodology discussed in Section 3.2. Each sample from the vessel was subjected to a cycle of 5 analyses in the instrument. A total of 13 variants of the silty sand sample were distinguished. For each sample variant I–XIII, 5 mini-sample vessels of that variant were extracted (an example set of 5 mini-sample vessels is shown in Figure 11a,b). In order to obtain a meaningful statistical sample for both variants of the silty sand with a silt and clay fraction of  $f_{Si+Cl,1} = 15.14\%$  and  $f_{Si+Cl,2} = 20.48\%$ , a cycle consisting of 5 analyses in the device was carried out. Finally, 650 analyses were carried out in the laser particle size analyzer.

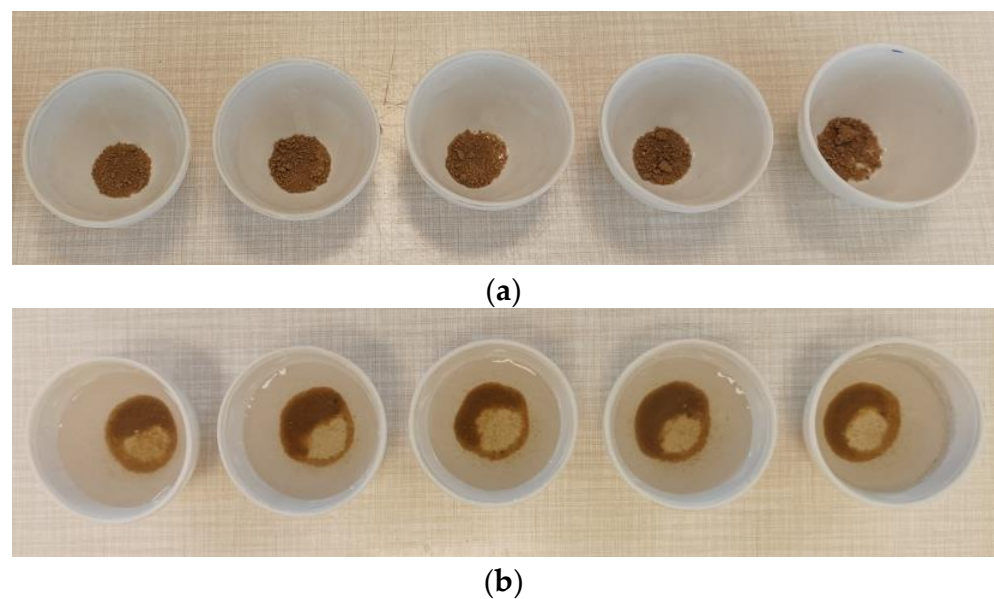


**Figure 11.** Preparation of silty sand samples for testing in laser particle size analyzer: (a) samples of silty sand before pouring distilled water (visible merged grains into compact lumps); (b) samples of silty sand after pouring distilled water and waiting for 24 h (separation into individual grains occurred).

#### 4. Test Results in the Laser Particle Size Analyzer

According to the description of the soil sample preparation process in Section 3.3, each variant of the silty sand sample was tested in the particle size analyzer by laser diffraction in five cycles for the extracted five mini-samples (a total of 25 tests performed for each variant I–XIII from Table 4). The 25 test results were averaged to present the results of the tests for each variant I–XIII (depending on the configuration of variables used: initial launcher pressure acting on the bar projectile  $p_1-p_2-p_3$  and moisture content of the soil sample  $w_1-w_2-w_3-w_4$ ) in summary graphs of grain size curves with reference to the reference sample:

- for the first type of soil sample— $f_{Si+Cl,1} = 15.14\%$ :
  - Figure 12a with variable configuration values  $w_1 = 0\%$  and  $p_1 = 1.2$  bar ( $v_1 = 12.76$  m/s)— $p_2 = 1.8$  bar ( $v_2 = 17.69$  m/s)— $p_3 = 2.4$  bar ( $v_3 = 21.32$  m/s);
  - Figure 12b with variable configuration values  $w_2 = 5\%$  and  $p_1 = 1.2$  bar ( $v_1 = 12.76$  m/s)— $p_2 = 1.8$  bar ( $v_2 = 17.69$  m/s)— $p_3 = 2.4$  bar ( $v_3 = 21.32$  m/s);
  - Figure 12c with variable configuration values  $w_3 = 10\%$  and  $p_1 = 1.2$  bar ( $v_1 = 12.76$  m/s)— $p_2 = 1.8$  bar ( $v_2 = 17.69$  m/s)— $p_3 = 2.4$  bar ( $v_3 = 21.32$  m/s);
  - Figure 12d with variable configuration values  $w_4 = 15\%$  and  $p_1 = 1.2$  bar ( $v_1 = 12.76$  m/s)— $p_2 = 1.8$  bar ( $v_2 = 17.69$  m/s)— $p_3 = 2.4$  bar ( $v_3 = 21.32$  m/s);

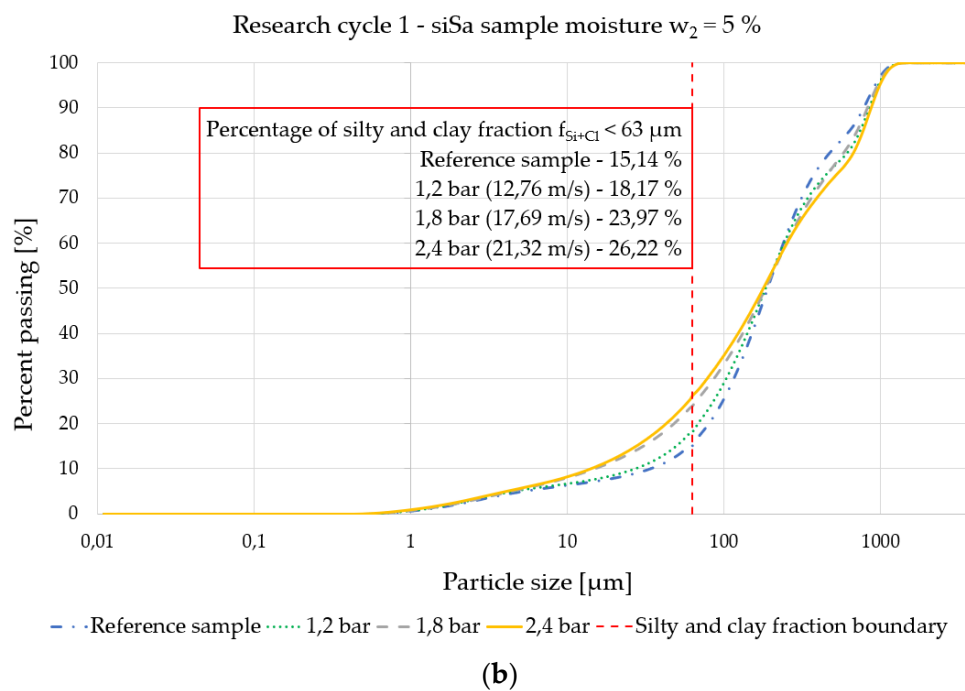
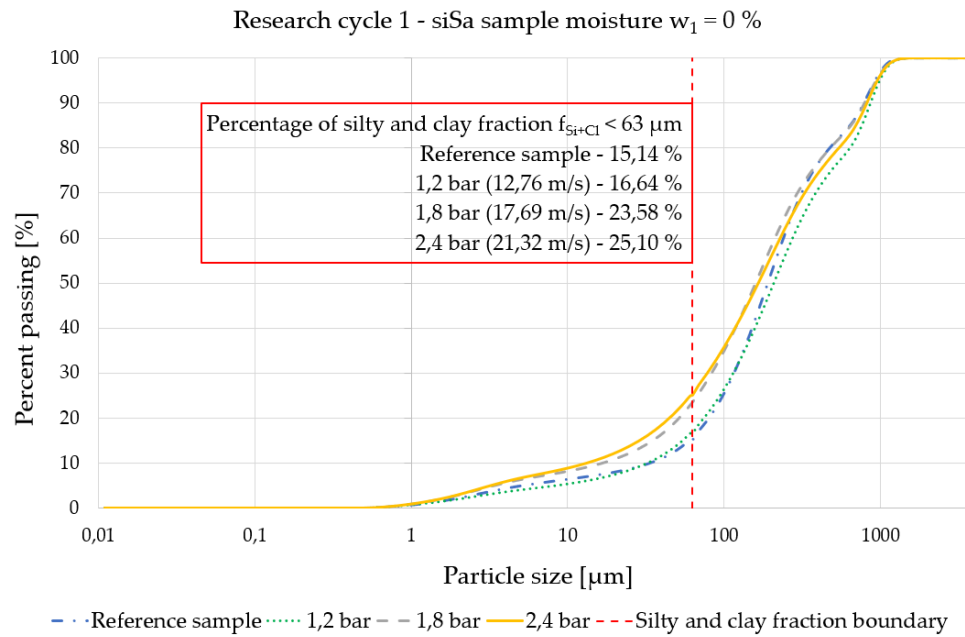
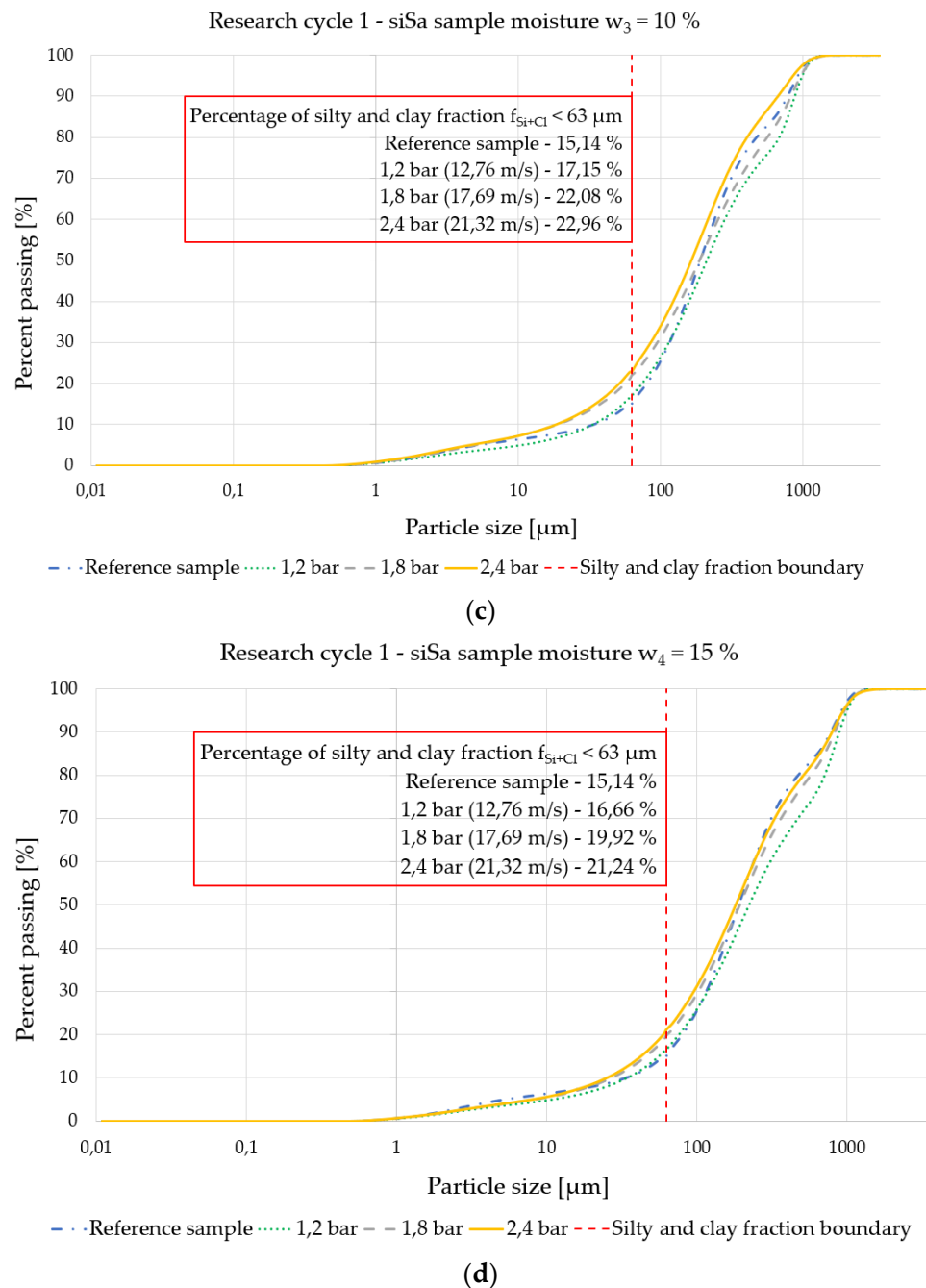


Figure 12. Cont.



**Figure 12.** Summary graphs of grain size curves for silty sand with silt and clay fraction  $f_{Si+Cl,1} = 15.14\%$  for sample variants I–XIII (12 sample variants subjected to dynamic impact in SHPB and reference sample without dynamic impact) in variable configurations: (a)  $w_1$  and  $p_1$  ( $v_1$ )– $p_2$  ( $v_2$ )– $p_3$  ( $v_3$ ), (b)  $w_2$  and  $p_1$  ( $v_1$ )– $p_2$  ( $v_2$ )– $p_3$  ( $v_3$ ), (c)  $w_3$  and  $p_1$  ( $v_1$ )– $p_2$  ( $v_2$ )– $p_3$  ( $v_3$ ), (d)  $w_4$  and  $p_1$  ( $v_1$ )– $p_2$  ( $v_2$ )– $p_3$  ( $v_3$ ).

- for the second type of soil sample— $f_{Si+Cl,2} = 20.48\%$ :
  - Figure 13a with variable configuration values  $w_1 = 0\%$  and  $p_1 = 1.2$  bar ( $v_1 = 12.76$  m/s)– $p_2 = 1.8$  bar ( $v_2 = 17.69$  m/s)– $p_3 = 2.4$  bar ( $v_3 = 21.32$  m/s);
  - Figure 13b with variable configuration values  $w_2 = 5\%$  and  $p_1 = 1.2$  bar ( $v_1 = 12.76$  m/s)– $p_2 = 1.8$  bar ( $v_2 = 17.69$  m/s)– $p_3 = 2.4$  bar ( $v_3 = 21.32$  m/s);
  - Figure 13c with variable configuration values  $w_3 = 10\%$  and  $p_1 = 1.2$  bar ( $v_1 = 12.76$  m/s)– $p_2 = 1.8$  bar ( $v_2 = 17.69$  m/s)– $p_3 = 2.4$  bar ( $v_3 = 21.32$  m/s);
  - Figure 13d with variable configuration values  $w_4 = 15\%$  and  $p_1 = 1.2$  bar ( $v_1 = 12.76$  m/s)– $p_2 = 1.8$  bar ( $v_2 = 17.69$  m/s)– $p_3 = 2.4$  bar ( $v_3 = 21.32$  m/s).

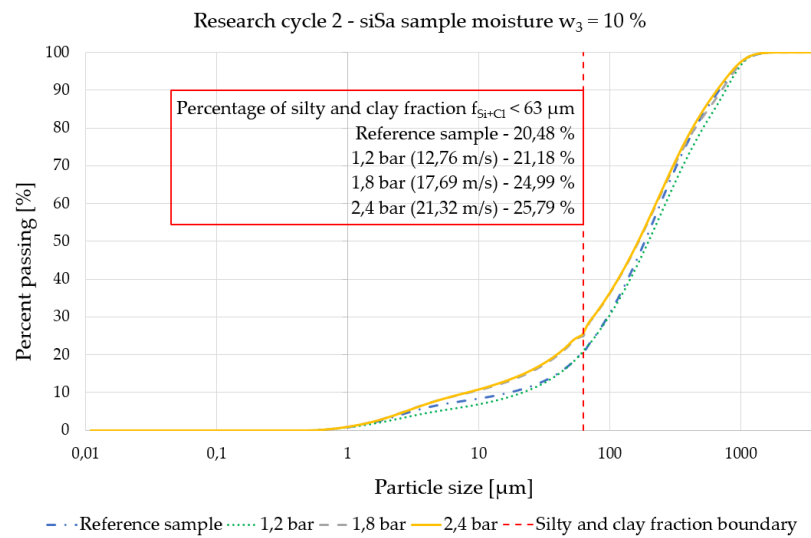
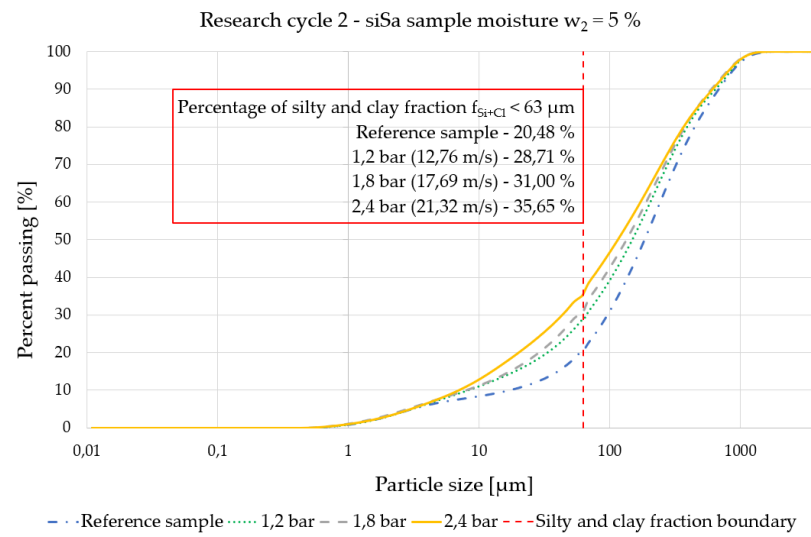
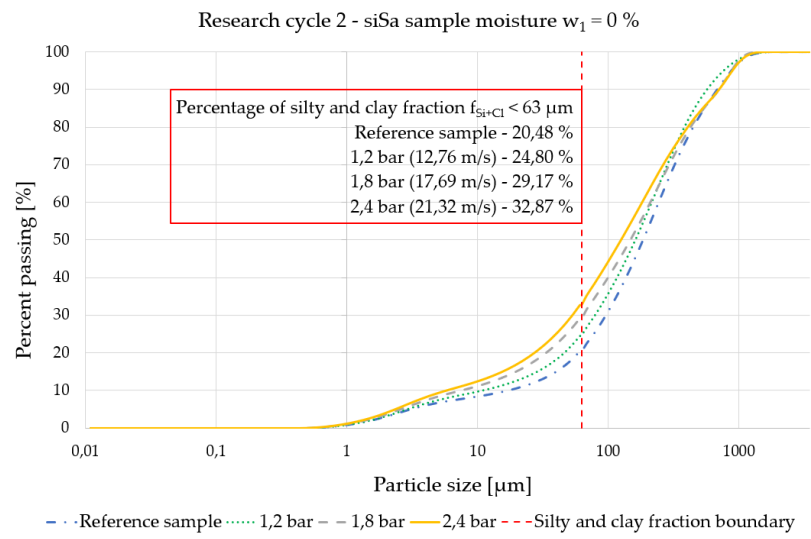
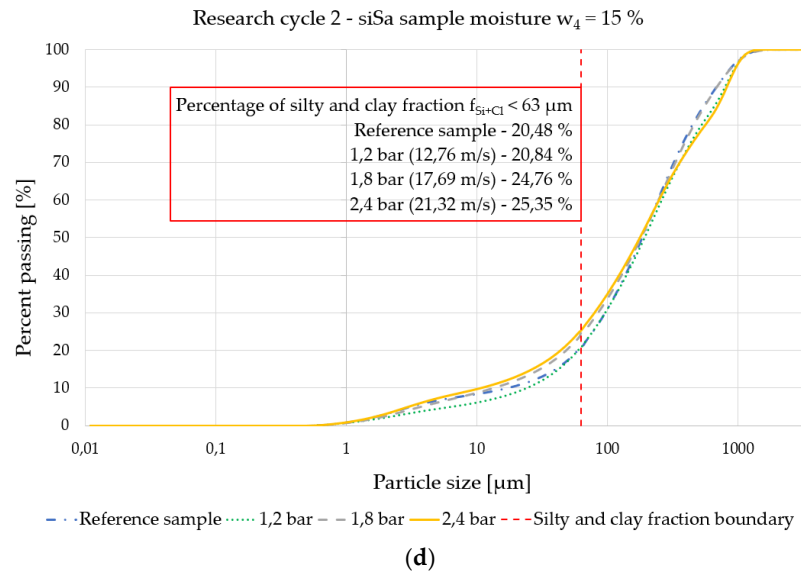


Figure 13. Cont.



**Figure 13.** Summary graphs of grain size curves for silty sand with silt and clay fraction  $f_{Si+Cl,2} = 20.48\%$  for sample variants I–XIII (12 sample variants subjected to dynamic impact in SHPB and reference sample without dynamic impact) in variable configurations: (a)  $w_1$  and  $p_1 (v_1)$ – $p_2 (v_2)$ – $p_3 (v_3)$ , (b)  $w_2$  and  $p_1 (v_1)$ – $p_2 (v_2)$ – $p_3 (v_3)$ , (c)  $w_3$  and  $p_1 (v_1)$ – $p_2 (v_2)$ – $p_3 (v_3)$ , (d)  $w_4$  and  $p_1 (v_1)$ – $p_2 (v_2)$ – $p_3 (v_3)$ .

**5. Discussion**

In order to clearly summarize the results of the tests in the laser particle size analyzer (results from Section 4) and to show the visible trends in the change of granulometric composition of the samples of silty sand subjected to dynamic impact in the SHPB test, Table 5 is prepared for both soil samples with initial content of silty and clay fraction  $f_{Si+Cl,1} = 15.14\%$  and  $f_{Si+Cl,2} = 20.48\%$ . The table summarizes the results taking into account the initial moisture content of the soil sample and the pneumatic launcher pressure of the SHPB loading bar projectile.

**Table 5.** Summary of  $f_{Si+Cl}$  silty and clay fraction values obtained in the laser particle size analyzer for the different configurations of the variable variants of the silty sand sample after dynamic impact in the SHPB test.

Reference Sample $f_{Si+Cl}$	Moisture Content of the Silty Sand Sample $w_i$					
		$w_1 = 0\%$	$w_2 = 5\%$	$w_3 = 10\%$	$w_4 = 15\%$	
$f_{Si+Cl,1} = 15.14\%$	Launcher pressure $p_i$ / Impact velocity $v_i$	$p_1 = 1.2$ bar $v_1 = 12.76$ m/s	$f_{Si+Cl,1-I} = 16.64\%$	$f_{Si+Cl,1-IV} = 18.17\%$	$f_{Si+Cl,1-VII} = 17.15\%$	$f_{Si+Cl,1-X} = 16.66\%$
		$p_2 = 1.8$ bar $v_2 = 17.69$ m/s	$f_{Si+Cl,1-II} = 23.58\%$	$f_{Si+Cl,1-V} = 23.97\%$	$f_{Si+Cl,1-VIII} = 22.08\%$	$f_{Si+Cl,1-XI} = 19.92\%$
		$p_3 = 2.4$ bar $v_3 = 21.32$ m/s	$f_{Si+Cl,1-III} = 25.10\%$	$f_{Si+Cl,1-VI} = 26.22\%$	$f_{Si+Cl,1-IX} = 22.96\%$	$f_{Si+Cl,1-XII} = 21.24\%$
$f_{Si+Cl,2} = 20.48\%$	Launcher pressure $p_i$ / Impact velocity $v_i$	$p_1 = 1.2$ bar $v_1 = 12.76$ m/s	$f_{Si+Cl,2-I} = 24.80\%$	$f_{Si+Cl,2-IV} = 28.71\%$	$f_{Si+Cl,2-VII} = 21.18\%$	$f_{Si+Cl,2-X} = 20.84\%$
		$p_2 = 1.8$ bar $v_2 = 17.69$ m/s	$f_{Si+Cl,2-II} = 29.17\%$	$f_{Si+Cl,2-V} = 31.00\%$	$f_{Si+Cl,2-VIII} = 24.99\%$	$f_{Si+Cl,2-XI} = 24.76\%$
		$p_3 = 2.4$ bar $v_3 = 21.32$ m/s	$f_{Si+Cl,2-III} = 32.87\%$	$f_{Si+Cl,2-VI} = 35.65\%$	$f_{Si+Cl,2-IX} = 25.79\%$	$f_{Si+Cl,2-XII} = 25.35\%$

Based on the data presented in Table 5, it is possible to note the behavioral trends and direction of trends in the dynamic characteristics of the silty sand:

- Each silty sand sample used on the SHPB test stand achieved a higher proportion of fine fractions (silt and clay) in its granulometric composition after the test compared to the reference sample. Each dynamic impact with the bar projectile resulted in an increase in the value of the silt and clay fraction  $f_{Si+Cl}$ —there was a phenomenon of destruction of the soil skeleton through grain breaking and an increase in the percentage of smaller-diameter grains. The correctness of Equations (4) and (5) can be seen:

$$f_{Si+Cl,1-I} \div f_{Si+Cl,1-XII} > f_{Si+Cl,1}; \tag{4}$$

$$f_{Si+Cl,2-I} \div f_{Si+Cl,2-XII} > f_{Si+Cl,2}. \tag{5}$$

- For a given moisture content of a soil sample, there was a trend towards an increase in the proportion of the silt and clay fraction in the granulometric composition with an increase in the initially applied pressure of the pneumatic launcher to start the bar projectile movement. The trend in the behavior of the sample occurred as the impact velocity of the bar projectile increased, which can be represented by Equations (6)–(9):

$$w_1 = 0\% \rightarrow \left( \begin{matrix} f_{Si+Cl,1-I} < f_{Si+Cl,1-II} < f_{Si+Cl,1-III} \\ f_{Si+Cl,2-I} < f_{Si+Cl,2-II} < f_{Si+Cl,2-III} \end{matrix} \right); \tag{6}$$

$$w_2 = 5\% \rightarrow \left( \begin{matrix} f_{Si+Cl,1-IV} < f_{Si+Cl,1-V} < f_{Si+Cl,1-VI} \\ f_{Si+Cl,2-IV} < f_{Si+Cl,2-V} < f_{Si+Cl,2-VI} \end{matrix} \right); \tag{7}$$

$$w_3 = 10\% \rightarrow \left( \begin{matrix} f_{Si+Cl,1-VII} < f_{Si+Cl,1-VIII} < f_{Si+Cl,1-IX} \\ f_{Si+Cl,2-VII} < f_{Si+Cl,2-VIII} < f_{Si+Cl,2-IX} \end{matrix} \right); \tag{8}$$

$$w_4 = 15\% \rightarrow \left( \begin{matrix} f_{Si+Cl,1-X} < f_{Si+Cl,1-XI} < f_{Si+Cl,1-XII} \\ f_{Si+Cl,2-X} < f_{Si+Cl,2-XI} < f_{Si+Cl,2-XII} \end{matrix} \right). \tag{9}$$

- As the moisture content of the soil sample increased, there was no simple relationship of change in the proportion of the silt and clay fraction in the granulometric composition (only an increasing relationship or only a decreasing relationship). For the moisture content of soil samples,  $w_1$  and  $w_2$  (values below the optimum moisture content  $w_{opt}$ ) for a given initial pressure of the pneumatic launcher (given impact velocity), a tendency towards an increase in the value of the silt and clay fraction was apparent (there was no significant effect of water on the test results). The higher the moisture content of the soil sample (in particular for  $w_3$  and  $w_4$  values above the optimum moisture content  $w_{opt}$ ), the stronger the trend of a decreasing value of the silt and clay fraction in the granulometric composition of the silty sand sample could be seen. There was a clear, dynamic response of the water filling the soil pores—the water gave the sample some characteristics of an elastic material and “damped” the dynamic impact of the bar projectile impact. This interaction had the effect of reducing the phenomenon of destruction of the soil skeleton by grain fracture, which can be represented in Equations (10)–(12):

$$\left( \begin{matrix} p_1 = 1.2 \text{ bar} \\ v_1 = 12.76 \text{ m/S} \end{matrix} \right) \rightarrow \left( \begin{matrix} \text{if } w_1 < w_2 < w_{opt,1} \text{ then } f_{Si+Cl,1-I} < f_{Si+Cl,1-IV} \\ \text{if } w_2 < w_{opt,1} < w_3 < w_4 \text{ then } f_{Si+Cl,1-IV} > f_{Si+Cl,1-VII} > f_{Si+Cl,1-X} \\ \text{if } w_1 < w_2 < w_{opt,2} \text{ then } f_{Si+Cl,2-I} < f_{Si+Cl,2-IV} \\ \text{if } w_2 < w_{opt,2} < w_3 < w_4 \text{ then } f_{Si+Cl,2-IV} > f_{Si+Cl,2-VII} > f_{Si+Cl,2-X} \end{matrix} \right); \tag{10}$$

$$\left( \begin{matrix} p_2 = 1.8 \text{ bar} \\ v_2 = 17.69 \text{ m/S} \end{matrix} \right) \rightarrow \left( \begin{matrix} \text{if } w_1 < w_2 < w_{opt,1} \text{ then } f_{Si+Cl,1-II} < f_{Si+Cl,1-V} \\ \text{if } w_2 < w_{opt,1} < w_3 < w_4 \text{ then } f_{Si+Cl,1-V} > f_{Si+Cl,1-VIII} > f_{Si+Cl,1-XI} \\ \text{if } w_1 < w_2 < w_{opt,2} \text{ then } f_{Si+Cl,2-II} < f_{Si+Cl,2-V} \\ \text{if } w_2 < w_{opt,2} < w_3 < w_4 \text{ then } f_{Si+Cl,2-V} > f_{Si+Cl,2-VIII} > f_{Si+Cl,2-XI} \end{matrix} \right); \tag{11}$$

$$\begin{pmatrix} p_3 = 2.4 \text{ bar} \\ v_3 = 21.32 \text{ m/S} \end{pmatrix} \rightarrow \begin{pmatrix} \text{if } w_1 < w_2 < w_{opt,1} \text{ then } f_{Si+Cl,1-III} < f_{Si+Cl,1-VI} \\ \text{if } w_2 < w_{opt,1} < w_3 < w_4 \text{ then } f_{Si+Cl,1-VI} > f_{Si+Cl,1-IX} > f_{Si+Cl,1-XII} \\ \text{if } w_1 < w_2 < w_{opt,2} \text{ then } f_{Si+Cl,2-III} < f_{Si+Cl,2-VI} \\ \text{if } w_2 < w_{opt,2} < w_3 < w_4 \text{ then } f_{Si+Cl,2-VI} > f_{Si+Cl,2-IX} > f_{Si+Cl,2-XII} \end{pmatrix}. \quad (12)$$

➤ Table 6 shows the percentage changes in silt and clay fraction as a consequence of bar projectile impact during the SHPB test compared to the reference sample, depending on the configuration of the variables—soil sample moisture content  $w_i$  and initial shot pressure  $p_i$  (impact velocity  $v_i$ ). For the first type of soil sample  $f_{Si+Cl,1} = 15.14\%$ , the bar projectile impact load was most significant at a launching pressure  $p_2 = 1.8$  bar for all moisture content variants  $w_1 \div w_4$  (particularly prominent values are for samples with moisture content  $w_1$  and  $w_2$  lower than the optimum moisture content  $w_{opt}$ —for moisture content  $w_3$  and  $w_4$  higher than the optimum moisture content  $w_{opt}$ , there is a phenomenon of “damping” of the impact through the reaction of water in the soil pores). At this pressure  $p_2$ , the greatest percentage change in granulometric composition occurred through an increase in the value of the silt and clay fraction in relation to the reference sample  $f_{Si+Cl,1}$ :

- $f_{Si+Cl,1} = 15.14\% \rightarrow f_{Si+Cl,1-III} = 25.10\%$  (increase of 9.96%);
- $f_{Si+Cl,1} = 15.14\% \rightarrow f_{Si+Cl,1-VI} = 26.22\%$  (increase of 11.08%);
- $f_{Si+Cl,1} = 15.14\% \rightarrow f_{Si+Cl,1-IX} = 22.96\%$  (increase of 7.82%);
- $f_{Si+Cl,1} = 15.14\% \rightarrow f_{Si+Cl,1-XII} = 21.24\%$  (increase of 6.10%).

However, for the second soil sample type  $f_{Si+Cl,2} = 20.48\%$ , the most significant was the bar projectile impact at SHPB pneumatic launcher pressure  $p_3 = 2.4$  bar for all moisture contents  $w_1 \div w_4$  (analogous to the first sample type, values were particularly noticeable for samples with moisture contents  $w_1$  and  $w_2$  lower than the optimum moisture content  $w_{opt}$ —for moisture contents  $w_3$  and  $w_4$  higher than the optimum moisture content  $w_{opt}$ , a phenomenon of “damping” of the impact occurred through the reaction of water in soil pores). At this pressure  $p_3$ , the greatest percentage change in granulometric composition occurred through an increase in the value of the silt and clay fraction in relation to the reference sample  $f_{Si+Cl,2}$ :

- $f_{Si+Cl,2} = 20.48\% \rightarrow f_{Si+Cl,2-III} = 32.87\%$  (increase of 12.39%);
- $f_{Si+Cl,2} = 20.48\% \rightarrow f_{Si+Cl,2-VI} = 35.65\%$  (increase of 15.17%);
- $f_{Si+Cl,2} = 20.48\% \rightarrow f_{Si+Cl,2-IX} = 25.79\%$  (increase of 5.31%);
- $f_{Si+Cl,2} = 20.48\% \rightarrow f_{Si+Cl,2-XII} = 25.35\%$  (increase of 4.87%).

**Table 6.** Summary of percentage changes in silt and clay fraction as a consequence of bar projectile impact during SHPB testing compared to the  $f_{Si+Cl}$  reference sample depending on the configuration of variables—moisture content of the soil sample  $w_i$  and initial impact pressure  $p_i$ .

Launcher Pressure $p_i$ / Impact Velocity $v_i$	Moisture Content of the Silty Sand Sample $w_i$ / Difference between $f_{Si+Cl,1-k}$ ( $f_{Si+Cl,2-k}$ ) and Reference $f_{Si+Cl,1}$ ( $f_{Si+Cl,2}$ )							
	$w_1 = 0\%$	$\Delta$ $f_{Si+Cl,1-k}$ — $f_{Si+Cl,1}$	$w_2 = 5\%$	$\Delta$ $f_{Si+Cl,1-k}$ — $f_{Si+Cl,1}$	$w_3 = 10\%$	$\Delta$ $f_{Si+Cl,1-k}$ — $f_{Si+Cl,1}$	$w_4 = 15\%$	$\Delta$ $f_{Si+Cl,1-k}$ — $f_{Si+Cl,1}$
	$p_1 = 1.2$ bar $v_1 = 12.76$ m/s	$f_{Si+Cl,1-I} = 16.64\%$	1.50%	$f_{Si+Cl,1-IV} = 18.17\%$	3.03%	$f_{Si+Cl,1-VII} = 17.15\%$	2.01%	$f_{Si+Cl,1-X} = 16.66\%$
$p_2 = 1.8$ bar $v_2 = 17.69$ m/s	$f_{Si+Cl,1-II} = 23.58\%$	8.44%	$f_{Si+Cl,1-V} = 23.97\%$	8.83%	$f_{Si+Cl,1-VIII} = 22.08\%$	6.94%	$f_{Si+Cl,1-XI} = 19.92\%$	4.78%
$p_3 = 2.4$ bar $v_3 = 21.32$ m/s	$f_{Si+Cl,1-III} = 25.10\%$	9.96%	$f_{Si+Cl,1-VI} = 26.22\%$	11.08%	$f_{Si+Cl,1-IX} = 22.96\%$	7.82%	$f_{Si+Cl,1-XII} = 21.24\%$	6.10%
		$\Delta$ $f_{Si+Cl,2-k}$ — $f_{Si+Cl,2}$		$\Delta$ $f_{Si+Cl,2-k}$ — $f_{Si+Cl,2}$		$\Delta$ $f_{Si+Cl,2-k}$ — $f_{Si+Cl,2}$		$\Delta$ $f_{Si+Cl,2-k}$ — $f_{Si+Cl,2}$
$p_1 = 1.2$ bar $v_1 = 12.76$ m/s	$f_{Si+Cl,2-I} = 24.80\%$	4.32%	$f_{Si+Cl,2-IV} = 28.71\%$	8.23%	$f_{Si+Cl,2-VII} = 21.18\%$	0.70%	$f_{Si+Cl,2-X} = 20.84\%$	0.36%
$p_2 = 1.8$ bar $v_2 = 17.69$ m/s	$f_{Si+Cl,2-II} = 29.17\%$	8.69%	$f_{Si+Cl,2-V} = 31.00\%$	10.52%	$f_{Si+Cl,2-VIII} = 24.99\%$	4.51%	$f_{Si+Cl,2-XI} = 24.76\%$	4.28%
$p_3 = 2.4$ bar $v_3 = 21.32$ m/s	$f_{Si+Cl,2-III} = 32.87\%$	12.39%	$f_{Si+Cl,2-VI} = 35.65\%$	15.17%	$f_{Si+Cl,2-IX} = 25.79\%$	5.31%	$f_{Si+Cl,2-XII} = 25.35\%$	4.87%

The four directions of behavioral trends in the dynamic characteristics of the silty sand discussed above are susceptible to the influence of experimental conditions. Special attention should be given to the issues:

- Parallelism of the contact surface between the soil sample-initiating bar and the transmitting bar. There is a particular risk of the parallelism condition not being achieved as a result of the compaction process of the soil sample. Silty sand is a loose material and susceptible to shape change. Applying the pressure plate elements in a way that is not perpendicular to the wall edge of the soil sample casing (rigid ring) will result in non-parallelism of the contact surface between the soil sample-initiating bar and transmitting bar (i.e., there will be a local air void). Consequently, incorrect waveform data will be recorded for the reflected wave (as a result of non-parallelism of the contact surface between soil sample-initiating bar) and transmitted wave (as a result of non-parallelism of the contact surface between the soil sample-transmitting bar).
- Cohesive effect resulting from the internal structure of the tested soil sample. Silty sand is not a pure representative of sand containing only grains with a diameter in the range of 0.063 mm–2 mm (according to Figure 1). Silty sand has fine fractions below the limit of 0.063 mm—these give the soil sample cohesive characteristics, and the cohesion value is not zero. In simplification, it can be assumed that the more the fine fraction, the higher the cohesion value. According to the data in Table 6, it can be seen that the cohesion effect is not the only important factor influencing the results—the pore water content of the soil should be taken into account.
- Interfacial friction effect is a widely discussed issue for the various materials tested in the SHPB test stand, particularly loose materials [61–63]. The incident wave created by the impact passes from the initiating bar to the soil sample during its propagation. The wave passes through a soil sample with a non-uniform and variable cross-section, which will result in an uneven stress distribution in the axial direction of the sample due to the interfacial friction effect.

## 6. Conclusions

This paper is concerned with the analysis of changes in the granulometric composition of silty sand samples through a procedure comparing the values of the silt and clay fraction  $f_{Si+Cl}$  in the structure before and after SHPB experiments using a laser diffraction particle size analyzer.

Two types of non-cohesive soil–silty sands were selected for testing. The optimum moisture contents  $w_{opt,1} = 8.70\%$  and  $w_{opt,2} = 9.20\%$  were determined for both reference samples (tests carried out using the Proctor method), and the silt and clay fractions  $f_{Si+Cl,1} = 15.14\%$  and  $f_{Si+Cl,2} = 20.48\%$  were determined (tests carried out using a laser diffraction particle size analyzer, assuming a boundary value of 63  $\mu\text{m}$  between the sandy fraction  $f_{Sa}$  and the silty fraction  $f_{Si}$ ).

During comparative analysis of the test results, repeatable trends in changes in the granulometric composition of soil samples were noted:

- Each dynamic impact with the bar projectile results in an increase in the value of the silt and clay fraction  $f_{Si+Cl}$  (there is a phenomenon of destruction of the soil skeleton through the breaking of grains and an increase in the percentage of grains with a smaller diameter).
- As the value of the initially applied pressure of the pneumatic launcher to start the bar projectile movement increases, there is a noticeable trend towards an increase in the proportion of the silt and clay fraction in the granulometric composition of the sample.
- For soil samples with a moisture content of  $w_1 = 0\%$  and  $w_2 = 5\%$  (values below the optimum moisture content of  $w_{opt,1} = 8.70\%$  and  $w_{opt,2} = 9.20\%$  depending on the type of sample) for a given initial pressure of the pneumatic launcher, a tendency towards an increase in the values of the silt and clay fraction is apparent (there is no significant

effect of water on the test results). The higher the moisture content of the soil sample (in particular for values  $w_3 = 10\%$  and  $w_4 = 15\%$  above the optimum moisture content  $w_{opt,1} = 8.70\%$  or  $w_{opt,2} = 9.20\%$  depending on the type of sample), the stronger the trend towards a decreasing value of the silt and clay fraction in the granulometric composition of the silty sand sample. There is a noticeable dynamic response of the water filling the soil pores—the water gives the sample the characteristics of an elastic material and “dampens” the dynamic impact of the bar projectile. This interaction of water in the sample has the effect of reducing the destruction of the soil skeleton through grain fracture.

- For the first type of soil sample  $f_{Si+Cl,1} = 15.14\%$ , the most significant is the bar projectile impact at an initial launcher pressure  $p_2 = 1.8$  bar for all sample moisture contents variants  $w_1 \div w_4$ —at this pressure  $p_2$ , the greatest percentage change in granulometric composition occurs through an increase in the value of the silty and clay fraction  $f_{Si+Cl,1-k}$  relative to the reference sample  $f_{Si+Cl,1}$ . On the other hand, for the second type of soil sample  $f_{Si+Cl,2} = 20.48\%$ , the greatest percentage change in granulometric composition occurs with a bar projectile impact at an initial launcher pressure  $p_3 = 2.4$  bar for all moisture content variants  $w_1 \div w_4$ —at this pressure  $p_3$ , the greatest percentage change in granulometric composition occurs through an increase in the value of the silty and clay fraction  $f_{Si+Cl,2-k}$  relative to the reference sample  $f_{Si+Cl,2}$ .

**Author Contributions:** Conceptualization, K.S.; methodology, K.S. and R.C.; formal analysis, K.S. and R.C.; investigation, K.S.; resources, K.S. and R.R.; data curation, K.S. and R.R.; writing—original draft preparation, K.S.; writing—review and editing, K.S., R.C. and L.K.; visualization, K.S.; supervision, R.C. and L.K. All authors have read and agreed to the published version of the manuscript.

**Funding:** This research received no external funding.

**Institutional Review Board Statement:** Not applicable.

**Informed Consent Statement:** Not applicable.

**Data Availability Statement:** Figure 5—<https://doi.org/10.37105/iboa.51> (Data available in a publicly accessible repository, accessed on 1 March 2023); Figure 8—<https://www.bettersizeinstruments.com/uploads/file/bettersizer-s3-plus-users-manual-v8.pdf> (Data available in a publicly accessible repository, accessed on 1 March 2023); Figure 9—<https://doi.org/10.37105/iboa.129> (Data available in a publicly accessible repository, accessed on 1 March 2023).

**Conflicts of Interest:** The authors declare no conflict of interest.

## Nomenclature

$w_i$	moisture content of soil sample—moisture variant no. $i$
$p_i$	pneumatic launcher pressures—pressure variant no. $i$
$v_i$	velocity of the bar projectile at the moment of impact with the initiating bar—velocity variant no. $i$
$w_{opt,i}$	optimum moisture content value—variant of soil sample type no. $i$
$f_{Si+Cl,i}$	content of fine fractions with a grain diameter of less than $63 \mu\text{m}$ (as the sum of silt and clay fractions)—variant of soil sample type no. $i$
$f_{Sa}$	sandy fraction content
$f_{Si}$	silty fraction content
$f_{Cl}$	clay fraction content
$\rho_{d,max}$	maximum volumetric density of the soil skeleton
$\epsilon^I$	incident wave generates deformations in the initiating bar
$\epsilon^T$	transmitted wave generates deformations in the transmitting bar
$\epsilon^R$	reflected wave generates deformations in the initiating bar
$L$	length of soil sample tested
$d$	diameter of soil sample tested
$\nu$	Poisson's ratio of soil sample tested

$f_{Si+Cl,i-k}$	content of fine fractions with a grain diameter of less than 63 $\mu\text{m}$ (as the sum of silt and clay fractions)—variant of soil sample type no. $i$ for the variant variables during experiment no. $k$
$\Delta f_{Si+Cl,i-k} - f_{Si+Cl,i}$	percentage change in granulometric composition through an increase in the value of the silty and clay fraction $f_{Si+Cl,i-k}$ relative to the reference sample $f_{Si+Cl,i}$

## References

- Kang, D.; Noh, H.-G.; Kim, J.; Lee, K. Inverse Identification of a Constitutive Model for High-Speed Forming Simulation: An Application to Electromagnetic Metal Forming. *Materials* **2022**, *15*, 7179. [[CrossRef](#)] [[PubMed](#)]
- Cieplak, K.; Janiszewski, J.; Grażka, M.; Konwerski, Ł. Planar Shear Specimens for High Strain-Rate Testing of Engineering Materials Using the Conventional SHPB Technique: Experimental and Numerical Studies. *Phys. Sci. Forum* **2022**, *4*, 13. [[CrossRef](#)]
- Brodova, I.; Yolshina, L.; Razorenov, S.; Rasposienko, D.; Petrova, A.; Shirinkina, I.; Shorokhov, E.; Muradymov, R.; Garkushin, G.; Savinykh, A. Effect of Grain Size on the Properties of Aluminum Matrix Composites with Graphene. *Metals* **2022**, *12*, 1054. [[CrossRef](#)]
- Wang, H.; Zhang, Y.; Tan, Z. Dynamic Response and Deformative Mechanism of the Shape Memory Polymer Filled with Low-Melting-Point Alloy under Different Dynamic Loads. *Polymers* **2023**, *15*, 423. [[CrossRef](#)] [[PubMed](#)]
- Lagdani, O.; Tarfaoui, M.; Rouway, M.; Laaouidi, H.; Sbai, S.J.; Amine Dabachi, M.; Aamir, A.; Nachtane, M. Influence of Moisture Diffusion on the Dynamic Compressive Behavior of Glass/Polyester Composite Joints for Marine Engineering Applications. *J. Compos. Sci.* **2022**, *6*, 94. [[CrossRef](#)]
- Hu, F.; Gao, J.; Zhang, B.; Qi, F.; Zhao, N.; Ouyang, X. Effects of Modified  $\text{Al}_2\text{O}_3$ -Decorated Ionic Liquid on the Mechanical Properties and Impact Resistance of a Polyurethane Elastomer. *Materials* **2021**, *14*, 4712. [[CrossRef](#)]
- Shi, B.; Xing, H.; Mu, C.; Li, J.; Xu, T.; Liu, W. Analysis of Optimal Loading Angle in Dynamic Flattened Brazilian Disc Splitting Test for Concrete. *Appl. Sci.* **2022**, *12*, 11834. [[CrossRef](#)]
- Guo, L.; Guo, R.; Yan, Y.; Zhang, Y.; Wang, Z.; Mu, Y. Dynamic Compression Mechanical Properties of Polyoxymethylene-Fiber-Reinforced Concrete. *Materials* **2022**, *15*, 7784. [[CrossRef](#)]
- Wang, W.; Zhang, Z.; Huo, Q.; Song, X.; Yang, J.; Wang, X.; Wang, J.; Wang, X. Dynamic Compressive Mechanical Properties of UR50 Ultra-Early-Strength Cement-Based Concrete Material under High Strain Rate on SHPB Test. *Materials* **2022**, *15*, 6154. [[CrossRef](#)]
- Zhang, K.; Wang, F.; Yang, B.; Li, L.; Gao, L.; Sun, Y.; Guo, F. Mechanical Response and Failure Mechanisms of Natural Bamboo Fiber Reinforced Poly-Benzoxazine Composite Subjected to Split-Hopkinson Tensile Bar Loading. *Polymers* **2022**, *14*, 1450. [[CrossRef](#)]
- Nachtane, M.; Tarfaoui, M.; Ledoux, Y.; Khammassi, S.; Leneveu, E.; Pelleter, J. Experimental Investigation on the Dynamic Behavior of 3D Printed CF-PEKK Composite under Cyclic Uniaxial Compression. *Compos. Struct.* **2020**, *247*, 112474. [[CrossRef](#)]
- Li, R.; Liu, L.; An, H.; Wang, Y. Study on Dynamic Constitutive Model of Polypropylene Concrete under Real-Time High-Temperature Conditions. *Appl. Sci.* **2022**, *12*, 1482. [[CrossRef](#)]
- Williams, O.; Taylor, S.; Lester, E.; Kingman, S.; Giddings, D.; Eastwick, C. Applicability of Mechanical Tests for Biomass Pellet Characterisation for Bioenergy Applications. *Materials* **2018**, *11*, 1329. [[CrossRef](#)]
- Bragov, A.M.; Iuzhina, T.N.; Lomunov, A.K.; Igumnov, L.A.; Belov, A.A.; Eremeyev, V.A. Investigation of Wood Properties at Elevated Temperature. *J. App. Comp. Mech.* **2022**, *8*, 298–305. [[CrossRef](#)]
- Kruszka, L.; Sobczyk, K. Applications of Hopkinson Bar Technique for Capability Testing of High-Energy Absorption Materials. In *NATO Science for Peace and Security Series C—Environmental Security*; Kovacs, T.A., Nyikes, Z., Furstner, I., Eds.; Springer: Berlin/Heidelberg, Germany, 2022. [[CrossRef](#)]
- Li, Z.; Zhu, Y.; Song, Q.; Wang, P.; Liu, D. Dynamic Mechanical Properties and Failure Characteristics of Sandstone with Pre-Flaws Parallel to the Loading Direction. *Sustainability* **2023**, *15*, 3587. [[CrossRef](#)]
- Zhou, J.; Zhao, G.; Meng, X.; Liu, C.; Ma, L.; Xu, W.; Cheng, X. Experimental Investigation of the Size Effect of Rock under Impact Load. *Minerals* **2023**, *13*, 43. [[CrossRef](#)]
- Wessling, A.; Kajberg, J. Dynamic Compressive and Tensile Characterisation of Igneous Rocks Using Split-Hopkinson Pressure Bar and Digital Image Correlation. *Materials* **2022**, *15*, 8264. [[CrossRef](#)] [[PubMed](#)]
- Wang, J.; Fan, P.; Wang, M.; Dong, L.; Ma, L.; Gao, L. Experimental study of one-dimensional compression creep in crushed dry coral sand. *Can. Geotech. J.* **2020**, *57*, 1854–1869. [[CrossRef](#)]
- Zhang, J.-C.; Li, Y.; Xu, B.; Meng, Q.-X.; Zhang, Q.; Wang, R.-B. Testing and constitutive modelling of the mechanical behaviours of gravelly soil material. *Arab. J. Geosci.* **2020**, *13*, 523. [[CrossRef](#)]
- Li, J.; Sun, W.; Li, Q.; Chen, S.; Yuan, M.; Xia, H. Influence of Layered Angle on Dynamic Characteristics of Backfill under Impact Loading. *Minerals* **2022**, *12*, 511. [[CrossRef](#)]
- Chmielewski, R.; Kruszka, L.; Rekucki, R.; Sobczyk, K. Experimental investigation of dynamic behavior of silty sand. *Arch. Civ. Eng.* **2021**, *LXVII*, 481–498. [[CrossRef](#)]
- Sobczyk, K.; Chmielewski, R.; Kruszka, L.; Rekucki, R. Strength Characterization of Soils' Properties at High Strain Rates Using the Hopkinson Technique—A Review of Experimental Testing. *Materials* **2022**, *15*, 274. [[CrossRef](#)]

24. Bhujangrao, T.; Froustey, C.; Iriondo, E.; Veiga, F.; Darnis, P.; Mata, F.G. Review of Intermediate Strain Rate Testing Devices. *Metals* **2020**, *10*, 894. [CrossRef]
25. Mishra, S.; Chakraborty, T.; Basu, D. High Strain Rate Stress-Strain Response of Soils—A Review. *Jpn. Geotech. Soc. Spec. Publ.* **2015**, *3*, 80–85. [CrossRef]
26. Web of Science Homepage. Available online: <https://www-1webofscience-1com-100003et80008.han.wat.edu.pl/wos/alldb/summary/> (accessed on 8 March 2023).
27. Springer Link Homepage. Available online: <https://link.springer.com/> (accessed on 8 March 2023).
28. Wu, N.; Fu, J.; Xiong, C. Studying the Characteristics of Chaos and Fractals of Construction Rocks under Different Loading Velocities. *Materials* **2022**, *15*, 7890. [CrossRef]
29. Wang, J.; Huang, L.; Li, X.; Wu, Y.; Liu, H. Effect of Particle Size Distribution on the Dynamic Mechanical Properties and Fractal Characteristics of Cemented Rock Strata. *Mathematics* **2022**, *10*, 2078. [CrossRef]
30. Wang, J.; Lei, L.; Liu, Y.; Yang, Y.; Huang, Y. Fracture Fractal and Energy Transfer Characteristics of Deep-Mine Marble under an Impact Load. *Minerals* **2023**, *13*, 275. [CrossRef]
31. Wang, H.; Xu, W.; Cheng, B.; Zong, Q. Research on Particle Size and Energy Consumption Law of Hard Coal Crushing under Impact Load Based on SHPB Test. *Appl. Sci.* **2023**, *13*, 3298. [CrossRef]
32. Yuan, Q.; Wang, L.; Xie, G.; Gu, S.; Khan, N.M.; Jiao, Z.; Liu, H. Evaluation of the Energy Consumption and Fractal Characteristics of Different Length-Diameter Ratios of Coal under Dynamic Impact. *Energies* **2022**, *15*, 5498. [CrossRef]
33. Waddoups, R.; Clarke, S.; Tyas, A.; Rigby, S.; Gant, M.; Elgy, I. An Approach to Quantifying the Influence of Particle Size Distribution on Buried Blast Loading. *Eng* **2023**, *4*, 319–340. [CrossRef]
34. Wang, T.; Ma, L.; Wang, M.; Li, Z.; Zhang, X.; Geng, H. Effects of particle shape on dynamic mechanical behaviours of coral sand under one-dimensional compression. *Eng. Geol.* **2022**, *304*, 106624. [CrossRef]
35. Li, S.A.; Xiong, Z.; Fan, P.; Xie, K. Experimental Study on the Influence of Moisture and Clay Content on Stress Wave Attenuation Characteristics of Filled Joints. *Appl. Sci.* **2022**, *12*, 9140. [CrossRef]
36. Yu, X.; Chen, L.; Fang, Q.; Chen, W. Stress Attenuation and Energy Absorption of the Coral Sand with Different Particle Sizes under Impacts. *Proceedings* **2018**, *2*, 545. [CrossRef]
37. Shemirani, A.B.; Naghdabadi, R.; Ashrafi, M.J. Experimental and numerical study on choosing proper pulse shapers for testing concrete specimens by split Hopkinson pressure bar apparatus. *Constr. Build. Mater.* **2016**, *125*, 326–336. [CrossRef]
38. Xu, D.; Zhang, Z.; Qin, Y.; Liu, T.; Cheng, Z. Effect of particle size distribution on dynamic properties of cemented coral sand under SHPB impact loading. *Soil Dyn. Earthq. Eng.* **2022**, *162*, 107438. [CrossRef]
39. Chen, H.; Zhang, C.; Wei, J.; Li, M.; Wang, Y. A modified method for estimating the stress state of granular materials in the passive confined pressure SHPB tests. *Int. J. Impact. Eng.* **2022**, *160*, 104063. [CrossRef]
40. Xu, D.; Zhang, Z.; Qin, Y.; Yang, Y. Effect of particle size on the failure behavior of cemented coral sand under impact loading. *Soil Dyn. Earthq. Eng.* **2021**, *149*, 106884. [CrossRef]
41. Chen, Y.; Tang, Y.; Guan, Y.; Liu, R.; Han, X.; Zhao, X. Study on the mechanical properties of coral sands with different particle gradations. *Mar. Georesources Geotechnol.* **2022**, *41*, 327–338. [CrossRef]
42. Chen, X.; Shen, J.; Wang, X.; Yao, T.; Xu, D. Effect of Saturation on Shear Behavior and Particle Breakage of Coral Sand. *J. Mar. Sci. Eng.* **2022**, *10*, 1280. [CrossRef]
43. *PN-EN ISO 14688-1*; Geotechnical Investigation and Research—Determination and Classification of Soils—Part 1: Determination and Description. ISO: Geneva, Switzerland, 2018.
44. *PN-EN ISO 17892-4:2017-01*; Geotechnical Investigation and Testing—Laboratory Testing of Soil—Part 4: Determination of Particle size Distribution. ISO: Geneva, Switzerland, 2017.
45. Wang, F.; Kong, L.; Zhou, Z. Study on Pore Structure and Mechanical Property of Expansive Soil under Different Dehydration Conditions. *Appl. Sci.* **2022**, *12*, 5981. [CrossRef]
46. Woldesenbet, T.T. Experimental Study on Stabilized Expansive Soil by Blending Parts of the Soil Kilned and Powdered Glass Wastes. *Adv. Civ. Eng.* **2022**, *2022*, 9645589. [CrossRef]
47. Al-Gharbawi, A.S.A.; Najemalden, A.M.; Fattah, M.Y. Expansive Soil Stabilization with Lime, Cement, and Silica Fume. *Appl. Sci.* **2023**, *13*, 436. [CrossRef]
48. Górska-Pawliczka, A. Frost heave—A challenge for road construction (in Polish). *Magazyn Autostrady.* **2017**, *5*, 116–122.
49. *PN-EN 13286-2*; Unbound and hydraulically bound mixtures—Part 2: Test methods for laboratory reference density and water content—Proctor compaction. CEN: Brussels, Belgium.
50. Sobczyk, K.; Chmielewski, R.; Kruszka, L. The concept of experimental research on the behavior of sand cover material for protective shelters for civilians. *Saf. Eng. Anthropog. Objects* **2020**, *1*, 11–16. [CrossRef]
51. Sobczyk, K.; Kruszka, L.; Chmielewski, R.; Rekućki, R. Performance characteristics of Hopkinson’s set-up pneumatic launcher. *Acta Polytech.* **2021**, *61*, 552–561. [CrossRef]
52. *ISO 13320*; Particle Size Analysis—Laser Diffraction Methods. ISO: Geneva, Switzerland, 2020.
53. *ISO 13322-2*; Particle Size Analysis—Image Analysis Methods—Part 2: Dynamic Image Analysis Methods. ISO: Geneva, Switzerland, 2021.
54. *ISO 9276-6*; Representation of Results of Particle Size Analysis—Part 6: Descriptive and Quantitative Representation of Particle Shape and Morphology. ISO: Geneva, Switzerland, 2008.

55. Bettersizer S3 Plus Laser Particle Size Analyzer User's Manual. Dandong Bettersize Instruments Ltd. Available online: <https://www.bettersizeinstruments.com/uploads/file/bettersizer-s3-plus-users-manual-v8.pdf> (accessed on 2 March 2023).
56. Lv, Y.; Liu, J.; Xiong, Z. One-dimensional dynamic compressive behavior of dry calcareous sand at high strain rates. *J. Rock Mech. Geotech. Eng.* **2019**, *11*, 192–201. [[CrossRef](#)]
57. Li, L.; Kuo, X.; Zhang, G.; Huang, K. Experimental Study on Dynamic Compressive Behaviors of Sand under Passive Confining Pressure. *Materials* **2022**, *15*, 4690. [[CrossRef](#)] [[PubMed](#)]
58. Wang, J.; Li, W.; Xu, L.; Du, Z.; Gao, G. Experimental study on pulse shaping techniques of large diameter SHPB apparatus for concrete. *Lat. Am. J. Solids Struct.* **2021**, *18*, 1. [[CrossRef](#)]
59. Konstantinov, A.; Bragov, A.M.; Igumnov, L.A.; Eremeyev, V.A.; Baladin, V.V.; Baladin, V.V. Experimental Study and Identification of a Dynamic Deformation Model of Dry Clay at Strain Rates up to 2500 s<sup>-1</sup>. *J. App. And Comp. Mech.* **2022**, *8*, 981–995. [[CrossRef](#)]
60. Sobczyk, K.; Kruszka, L.; Grązka, M.; Chmielewski, R.; Rekucki, R. Preparation of the non-cohesive soil sample and calibration of the pneumatical launcher in the dynamic soil test SHPB. *Saf. Eng. Anthropol. Objects* **2022**, *1*, 16–27. [[CrossRef](#)]
61. Pei, P.; Pei, Z.; Tang, Z. Numerical and Theoretical Analysis of the Inertia Effects and Interfacial Friction in SHPB Test Systems. *Materials* **2020**, *13*, 4809. [[CrossRef](#)] [[PubMed](#)]
62. Lu, F.; Lin, Y.; Wang, X.; Lu, L.; Chen, R. A theoretical analysis about the influence of interfacial friction in SHPB tests. *Int. J. Impact Eng.* **2015**, *79*, 95–101. [[CrossRef](#)]
63. Yu, X.; Zheng, B.; Yang, B.; Shi, T. Correction method of SHPB experiment considering adiabatic deformation and interfacial friction effects. *J. Aerosp. Power* **2018**, *33*, 2367–2375. [[CrossRef](#)]

**Disclaimer/Publisher's Note:** The statements, opinions and data contained in all publications are solely those of the individual author(s) and contributor(s) and not of MDPI and/or the editor(s). MDPI and/or the editor(s) disclaim responsibility for any injury to people or property resulting from any ideas, methods, instructions or products referred to in the content.